To Hydrogen Bond or Halogen Bond?

That is the Question

Hayden Robinson

Supervisor : Dr Duncan A. Wild

Honours Thesis submitted as part of the B.Sc. (Hons) degree

The School of Molecular Sciences

The University of Western Australia

Date of Submission: 23 October 2020

Declaration

I certify that the material of this thesis has not been submitted for any other award or degree at any institution.

To the best of my knowledge, any sources used in this thesis and any help received have been acknowledged within this thesis.

Hayden Robinson, 23/10/2020

Acknowledgements

I would first like to thank my supervisor, Duncan Wild, for the help and guidance that he has provided throughout the year. This project has been a very enjoyable and valuable experience that I will remember for years to come.

To the other Wild lab members, Peter Watson, Tim Corkish, and Christian Haakansson. Thanks for not only assisting me with learning the ropes of programs like Gaussian09 and CFOUR, but for also keeping the lab a fun and easygoing place to work in. All the banter, as well as the many stories that the three of you have told me about have been very entertaining.

Lastly, I would like to thank my family. Even though you may not really understand what I do, you were always there to listen to me talk about my project.

This research was undertaken with the assistance of computational resources from the Pople high-performance computing cluster of the Faculty of Science at the University of Western Australia.

Abstract

Gas-phase van der Waals clusters of halide chloromethane complexes have been studied both experimentally and computationally. Photoelectron spectra have been recorded for bromide complexes with dichloromethane, trichloromethane, and tetrachloromethane, while high level *ab initio* calculations have been performed on halide chloromethane complexes to complement experimental data. The intermolecular interactions that arise in these complexes are rationalised in terms of hydrogen and halogen bonding.

Contents

List of Figures

Chapter 1

Introduction

Intermolecular interactions between systems involving two or more molecules, or between a molecule and some other constituent such as an ion, play a fundamental role in chemistry. This project aims to further our understanding of intermolecular interactions by exploring systems involving halogens and chloromethanes, and investigating the hydrogen bonding and halogen bonding interactions that may arise. The following chapter will outline the background and theory of intermolecular interactions, and why they are important in the context of atmospheric chemistry.

1.1 Atmospheric Chemistry

Halogens are known to play a role in atmospheric chemistry. They tend to enter the troposphere and stratosphere due to natural events such as volcanic eruptions(1) and sea spray(2), or as a result of anthropogenic emissions such as chlorofluorocarbons(3). Ozone depletion in the stratosphere is known to be catalysed by halogen radicals(4) shown in equations 1.1 and 1.2 to give a net loss of ozone in equation 1.3, where X = Cl, Br or I.

$$X^{\bullet} + O_3 \longrightarrow XO^{\bullet} + O_2 \tag{1.1}$$

$$XO^{\bullet} + O \longrightarrow X^{\bullet} + O_2 \tag{1.2}$$

$$O_3 + O \longrightarrow 2O_2 \tag{1.3}$$

In terms of anthropogenic emissions, the source of such halogen radicals often originates from photodissociation reactions of simple halogenated molecules. Bromine radicals for instance, are formed from photodissociation of molecules like dibromomethane and tribromomethane(5). Similarly, iodine radicals can form from photodissociation of molecules like iodomethane and iodoethane(6). These halogen sources play an important role in the experimental method of this project.

1.1.1 Chloromethanes

The chloromethanes are amongst the simplest halogenated molecules, and are often used in the laboratory as chemical solvents. The four chloromethanes (CH_3Cl, CH_2Cl_2, $CHCl_3$ and CCl_4) can also be found in the atmosphere, and contribute to the release of chlorine radicals that deplete ozone. Tetrachloromethane is relatively inert, and has an estimated lifespan in the atmosphere of 33 years, while monochloromethane, dichloromethane, and trichloromethane have much shorter lifespans at 0.4-1.0 years(7). The much shorter lifespan is due to their high reactivity with hydroxyl radicals, shown in equation 1.4, where RH = CH_3Cl, CH_2Cl_2, or $CHCl_3$.

$$RH + OH^{\bullet} \longrightarrow R^{\bullet} + H_2O \tag{1.4}$$

Chloromethanes make for a good chlorine donor species as shown in equation 1.5, where a generic chloromethane RCl undergoes a photodissociation reaction. This gives the chlorine radical, which can proceed to react with ozone in equation 1.1. Note that the $R^\bullet$ products are not necessarily equivalent between equations 1.4 and 1.5.

$$\mathrm{RCl} + h\nu \longrightarrow \mathrm{R}^\bullet + \mathrm{Cl}^\bullet \tag{1.5}$$

1.2 Van der Waals Clusters

When studying chemical reactions, a potential energy surface is a representation of the conversion of reactants to products. On such a surface, there are also other species worth considering. While reactants and products are represented by local minima on a potential energy surface, transition structures are denoted by first order saddle points, and act as a barrier height to the reaction(8). Pre-reaction and post-reaction adducts may also be found on a potential energy surface. These adducts can also be referred to as van der Waals clusters, and are essentially molecules interacting with other molecules, ions or atoms to form a loosely bound complex. Such clusters can be formed in the gas-phase, and are important in the study of atmospheric chemistry, due to the large number of gas-phase particles in the troposphere and stratosphere constantly interacting with one another to form complexes. Van der Waals clusters are known to interact via intermolecular forces, like for instance what is seen in hydrogen bonding(9).

1.2.1 Hydrogen Bonding

Hydrogen bonding occurs when a hydrogen atom on a molecule interacts non-covalently with a more electronegative atom, such as nitrogen, oxygen, or a halogen. The main factor of this interaction is due to electrostatic effects, where the electronegative atom is electron dense, while the hydrogen is electron deficient. As a result, the hydrogen interacts with a lone pair of electrons on the electronegative atom. However, hydrogen bonding is not purely an electrostatic interaction.

Dispersion effects account for the movement of electrons producing small induced dipoles(10). Induction refers to an unequal sharing of electrons between two different atoms, where a more electronegative atom will pull electron density away from a less electronegative atom. Charge transfer is the transfer of a lone pair electron from the highest occupied atomic orbital of an electronegative atom A, to the σ^* antibonding lowest unoccupied molecular orbital of R-H(11), as was originally hypothesised by Mulliken(12). Pauli repulsion refers to the steric repulsive forces that arise when occupied orbitals overlap between the two reactants(11). This repulsion can be explained by the Pauli exclusion principle(13), where no two electrons can share the same quantum state and spin. In the event that overlapping orbitals do contain two electrons of the same quantum state and spin, they will repel one another. Hydrogen bonding is therefore a combination of electrostatic effects, charge transfer, dispersion effects and induction effects all playing a role in stabilising the bond, while Pauli repulsion acts as a destabilising factor(14,15).

1.2.2 Halogen Bonding

Halogen bonding occurs when a halogen interacts with the negative region of a nucleophile. Like hydrogen bonding, it is a non-covalent interaction that arises from electrostatic effects. A phenomenon known as the σ-hole(16) allows the interaction to take place, which is a region of low electron density along the R-X bond, where X is a halogen. A small dipole moment, with the positive end situated at the halogen, allows a nucleophilic species to form a complex with said halogen at an angle of 160-180° to the R-X bond(17). In contrast, an electrophilic species has been shown to interact with the halogen, but at an angle of 90-120° to the R-X bond(17). Halogen bonding is actually a subset of σ-hole bonding, as the chalcogens (group 16 elements), pnictogens (group 15 elements), and tetrels (group 14 elements) have all been shown to exhibit the σ-hole phenomenon(16).

The magnitude of the σ-hole is affected by electronegativity and by inductive effects(18). If the -R group on the halogen is highly electron withdrawing, then the magnitude of the σ-hole increases. Iodine forms the strongest halogen bonds because electron density is most easily pulled away from it, unlike fluorine which is highly electronegative and forms the weakest halogen bonds(19). Similar to hydrogen bonding, other factors affect the strength and stability of the halogen bond, which includes the charge transfer of a lone pair electron to the σ^* antibonding orbital of R-X. Dispersion effects and Pauli repulsion also play a role in the stability of the bond(15).

With the many similarities between hydrogen bonding and halogen bonding, it is not a surprise that the strength of a halogen bond can be comparable to the strength of a hydrogen bond(20,21). Hence, the formation of gas-phase van der Waals clusters of chloromethanes are studied to answer the question proposed in the project's title; to hydrogen bond or halogen bond?

1.3 Experimental Techniques

While there are various methods of examining van der Waals clusters experimentally, only two will be utilised in this project. Mass spectrometry and anion photoelectron spectroscopy are the two techniques that will be briefly discussed.

1.3.1 Mass Spectrometry

Mass spectrometry (MS) is a method of separating ions based on their mass to charge ratio (m/z). For investigation of anion van der Waals clusters, MS has been previously used in one of two ways. One method is to directly measure physical properties of the clusters from the mass spectrum itself. This can include thermochemical properties such as enthalpy, entropy, and Gibbs free energy(22). Thermochemical properties are useful because they can characterise a reaction in terms of a potential energy surface, as well as determine dissociation energies for clusters. Other various studies have used MS to investigate the kinetics of gas-phase clusters, such as through the determination of rate constants(23).

The other method that MS is used for is as a mass selection technique. Van der Waals clusters of a specific m/z can be chosen, and studied through another technique that is coupled to the mass spectrometer. Photoelectron spectroscopy is one such technique that has been widely used(24-26), as the electronic structure of van der Waals clusters can be characterised.

1.3.2 Photoelectron Spectroscopy

Photoelectron spectroscopy (PES) is the study of electron detachment from a chemical system as a result of an interaction with a photon. X-ray photons have enough energy to detach core electrons, while UV photons only have enough energy to detach valence electrons. If the detached electron originated from a negatively charged species, then this is known as anion PES. Through this method, the energy levels of neutral gas-phase van der Waals clusters ($\mathrm{A}\cdots\mathrm{B}$) can be determined by the photodetachment of an electron from their respective anion species ($\mathrm{A}^-\cdots\mathrm{B}$). The electron affinity (EA) of helium was determined in one of the first studies to utilise anion PES(27).

A photoelectron spectrum measures the amount of energy required to detach an electron from a chemical species. This is known as the electron binding energy (e_{BE}), which is calculated using the electron kinetic energy (e_{KE}) as well as the photon energy $h\nu$ (equation 1.6). The kinetic energy can be determined based on the mass of the electron (m_e), and the velocity of the detached electron (equation 1.7).

$$e_{\mathrm{BE}} = h\nu - e_{\mathrm{KE}} \tag{1.6}$$

$$e_{\mathrm{KE}} = \frac{1}{2} m_e v^2 \tag{1.7}$$

A diagram of the potential energy surfaces of the anion and neutral species are shown in Figure 1.1. The vertical detachment energy (VDE) represents the most likely electronic transition that will occur when an electron is detached from the anion, which corresponds to the largest binding energy peak, as explained by the Franck-Condon principle(28). For halogens, the largest peak is the ${}^2P_{3/2}$ electronic state, while a second, smaller peak corresponds to the ${}^2P_{1/2}$ electronic state.

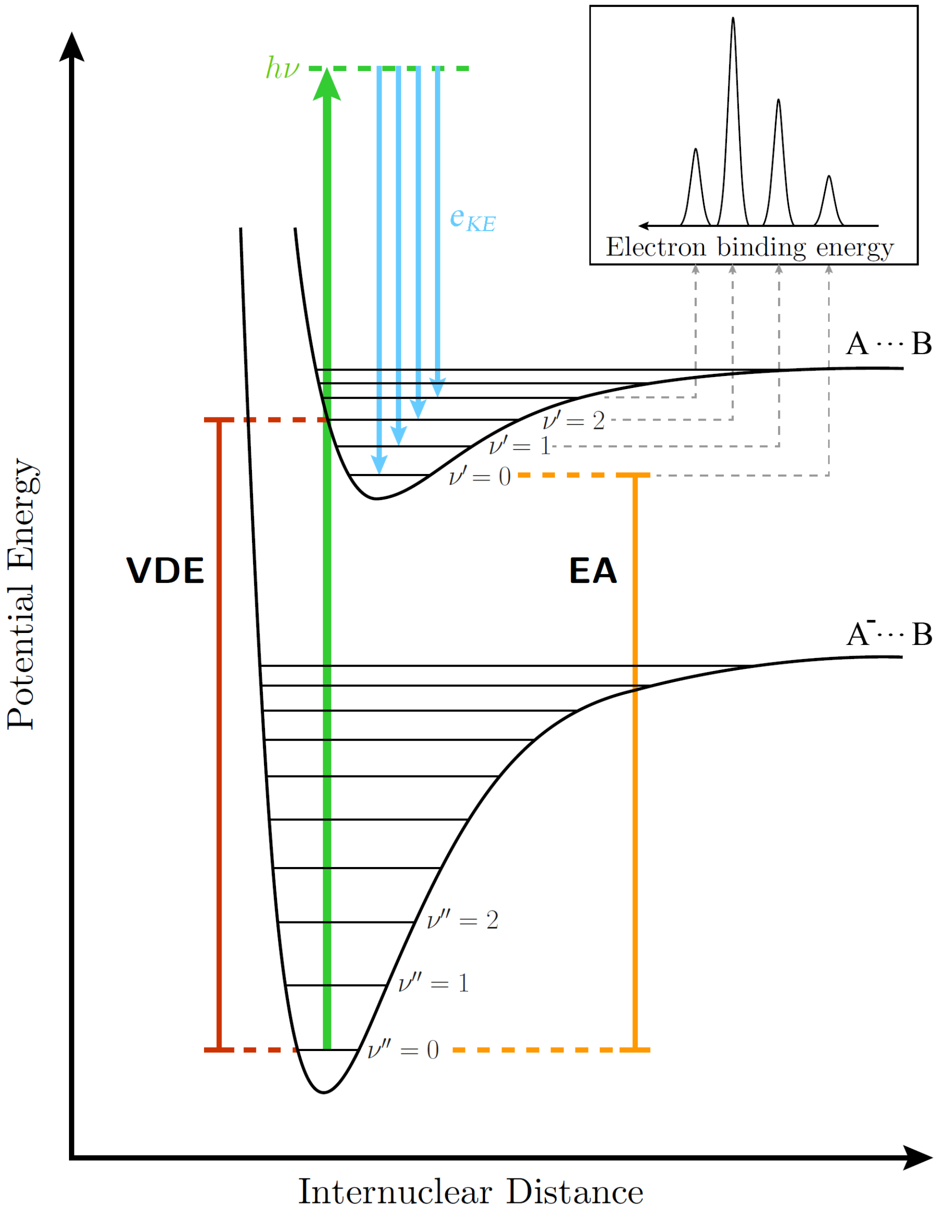

Figure 1.1: Photodetachment electronic transitions in anion PES(29).

1.4 Computational Chemistry

Computational chemistry is a theoretical approach to characterising chemical systems. Using quantum mechanics, it is possible to predict various properties of a system. This can include geometries, single point energies, and vibrational mode frequencies. Such calculations are utilised in this project to complement experimental data.

Ab initio calculations are one such method of theoretically characterising a chemical system. These calculations are based on first principles, only utilising fundamental constants. *Ab initio* methods involve approximating the non-relativistic, many-body, time independent Schrödinger equation, shown in equation 1.8.

$$\hat{H}\Psi = E\Psi \tag{1.8}$$

$\hat{H}$ refers to the Hamiltonian operator, which can be separated into kinetic energy and potential energy operators, as shown in equation 1.9. The kinetic energy operator can then be further separated into nuclei and electron kinetic energy, while the potential energy operator is separated into electron-nuclei attraction, nuclei-nuclei repulsion and electron-electron repulsion operators (equation 1.10). The Born-Oppenheimer approximation is then applied, which assumes that nuclei remain stationary relative to electrons due to the large mass difference, which allows the Schrödinger equation to be approximated in terms of electronic energy(30). Therefore, the $\hat{T}_N$ operator cancels to zero, and the remaining operators are expanded as shown in equation 1.11.

$$\hat{H} = \hat{T} + \hat{V} \tag{1.9}$$

$$\hat{H} = \hat{T}_N + \hat{T}_e + \hat{V}_{eN} + \hat{V}_{NN} + \hat{V}_{ee} \tag{1.10}$$

$$\hat{H} = -\frac{1}{2}\sum_{i=1}^{N}\nabla_i^2 - \sum_{i=1}^{N}\sum_{A=1}^{M}\frac{Z_A}{|r_i - R_A|} + \frac{1}{2}\sum_{\substack{A,B \\ A\neq B}}^{M}\frac{Z_A Z_B}{|R_A - R_B|} + \frac{1}{2}\sum_{\substack{i,j \\ i\neq j}}^{N}\frac{1}{|r_i - r_j|} \tag{1.11}$$

In the above equation, Z_A is the atomic number of nuclei A, R_A is the position of nuclei A, and r_i is the position of electron i. When the Hamiltonian operator acts on a wavefunction Ψ, an eigenvalue E is returned as a function of the nuclear coordinates (equation 1.12). This is an important result, because it forms the basis for the potential energy surface.

$$E = E(\mathbf{R}_1, \mathbf{R}_2, \ldots, \mathbf{R}_M) \tag{1.12}$$

1.4.1 Computational Theory

Hartree-Fock (HF) theory is the simplest *ab initio* method. It was one of the first methods developed to approximate the Schrödinger equation for multi-electron systems. HF theory makes two different approximations. The first is that the wavefunction is approximated by a single Slater determinant, where each electron occupies its own individual orbital(31). The second approximation is that all electrons in the system move independently through an average potential field(32). However, this second approximation gives rise to an issue, in that it does not account for electron correlation energy. Electron correlation energy (E_{corr}) refers to electron repulsion. It is the difference between the 'true' energy (E), which is the eigenvalue calculated from the non-relativistic, time independent, Born-Oppenheimer approximated Schrödinger equation, and the energy calculated from HF theory (E_{HF}) (shown in equation 1.13). A number of post-HF methods were created to account for electron correlation, and to improve on HF theory.

$$E_{corr} = E - E_{HF} \tag{1.13}$$

Møller-Plesset perturbation theory is one method that accounts for electron correlation. This is achieved by considering the unperturbed Hamiltonian operator (HF theory) as the zeroth-order approximation to the true Hamiltonian operator. From there, a small perturbation term is added, which represents electron-electron interactions. A power series of the perturbation term and unperturbed Hamiltonian can then be taken. The first-order perturbation cancels to zero, however the second-order perturbation has non-zero components, and thus can be added to the HF energy as a corrective term. This forms the basis for second-order Møller-Plesset perturbation theory (MP2)(33). MP2 has been shown to account for on average (92.4±4.6)% of electron correlation energy relative to QCISD(T) energy(34), and it is possible to go to higher orders to account for additional electron correlation such as third-order (MP3) or fourth-order (MP4). However, one downside of MP2 is that it is known to underestimate the ground state energy(35,36).

Coupled cluster (CC) theory is another method that accounts for electron correlation. The coupled cluster wavefunction is shown in equation 1.14. Expanding the exponential operator results in a Taylor series as a function of the cluster terms T_n, where n is the number of virtual excitations(37).

$$\Psi_{CC} = \exp(T)\Phi_0 \tag{1.14}$$

CC theory is one of the most accurate *ab initio* methods, as given enough excitations (and with a complete basis set), the power series will converge towards the 'exact solution', known as the full configuration-interaction (FCI) method(38). However, due to computational costs, this project will only consider coupled cluster theory with single, double, and perturbative triple excitations (CCSD(T)). Despite this, CCSD(T) is known to yield very accurate results, where the intrinsic error between the computational and experimental result is less than chemical accuracy (≈4.2 kJ mol^{-1})(39).

1.4.2 Basis Sets

A basis set is a set of functions that are applied to a one-electron space to simulate molecular orbitals. Slater type orbitals (STOs) were originally used to explain the radial components of orbitals(40), however full Slater-type calculations were very time consuming(41), and so Gaussian-type orbitals (GTOs) were introduced. While GTOs simulate the radial components of STOs well, they do not appropriately simulate electrons approaching a radius $r = 0$ from the nucleus. This is where the idea of primitive Gaussian functions comes from, which are linear combinations of GTOs that more accurately simulate STOs, and decrease calculation runtime.

The number of Gaussian functions used varies depending on the basis set. For example, STO-nG basis sets are minimal basis sets designed for first row elements, where one STO is replaced with n Gaussian functions. Both core, and valence orbitals (1s, 2s, 2p) are simulated by n Gaussian functions(41). A basis set such as 6-21G introduces what is known as split-valence. In this case, the core orbital (1s) is simulated by one basis function of six Gaussian functions, while each valence orbital (2s, 2p) is simulated by two basis functions. The inner valence is comprised of two Gaussian functions, and the outer valence is comprised of one Gaussian function(39). This is essentially a double zeta basis set, since two basis functions are used to simulate the valence orbitals. Increasing the number of valence basis functions increases the accuracy of the calculations.

There are other types of functions used in basis sets that improve accuracy. Diffuse functions are Gaussian functions with small exponent terms(42). They are important for improving accuracy on calculations involving very electronegative atoms, anions(43), and van der Waals complexes(44). In a basis set, the '+' notation represents the inclusion of s-type and p-type diffuse functions for first and second row elements, while ‘++’ refers to additional s-type diffuse functions for hydrogen atoms. For heavier atoms, d-type and f-type diffuse functions can also be included. Polarisation functions are added to account for unequal sharing of electrons between two atoms. This is achieved by addition of p-type polarisation functions to account for hydrogen (‘**’ or ‘p’ notation), and addition of d-type polarisation functions to account for non-hydrogen atoms (‘*’ or ‘d’ notation)(45).

Pseudopotentials can be used to decrease the number of electron interactions that need to be simulated in calculations involving heavy atoms. This is achieved by replacing electrons in core orbitals with an effective core potential (ECP), so that only valence electrons need to be treated explicitly in a calculation(46). This is advantageous, as it simplifies the calculation and hence decreases the overall computation time.

1.5 Previous Studies

Recently, a study by the Wild group showed the first experimental evidence of the structure of the $Cl^- \cdots CCl_4$ anion complex in the gas-phase(47). Evidence of the complex was found using MS, while PES was performed on the anion complex resulting in a photoelectron peak at 4.22 eV that corresponds to the $^2P_{3/2}$ state of the neutral complex. High level calculations at CCSD(T)/CBS theory confirmed that the halogen bonded $Cl^- \cdots CCl_4$ cluster was indeed the complex that was detected by PES. From this, it was concluded that the halogen bonded $Cl^- \cdots CCl_4$ anion complex is the most likely of two possible structures to be observed experimentally.

In terms of other halogen chloromethane complexes, there have been multiple computational studies. One study by the Glukhovtsev group focused on S_N2 reactions(48). Geometry optimisations were performed at MP2/6-31+G(d) theory, while single point energies were scaled up to QCISD(T)/6-311+G(3df,2p). Geometries and single point energies were found for $F^- \cdots CH_3Cl$, $Br^- \cdots CH_3Cl$ and $I^- \cdots CH_3Cl$, however these interactions only account for the halide hydrogen bonding with the chloromethane system, and not for a halogen bond interaction.

A study by the Kobychev group focused on the S_N2 reactions of chloromethane and tetrachloromethane with iodide and chloride anions(49). This study performed calculations at HF/3-21G* theory. Geometries were optimised for the $I^- \cdots CH_3Cl$, $Cl^- \cdots CH_3Cl$, $I^- \cdots CCl_4$ and $Cl^- \cdots CCl_4$ complexes, and energy profiles were characterised for the relevant reactions. However, these calculations are at a low level of theory, and thus the accuracy can be improved upon.

The Hiraoka group incorporated both experimental and computational methods in their studies on chloride chloromethane complexes(50). The geometry optimisations were run at B3LYP/6-31+G* theory, while single point energies were scaled up to QCISD(T)/6-311+G(d,p) theory. Experimental enthalpy changes for the formation of the chloride chloromethane complexes were found for $Cl^- \cdots CH_3Cl$, $Cl^- \cdots CH_2Cl_2$, $Cl^- \cdots CHCl_3$, and $Cl^- \cdots CCl_4$. Other studies using various MS techniques have experimentally determined the hydrogen bond strengths of halide chloromethanes complexes, such as Giles and Grimsrud studied the $Cl^- \cdots CHCl_3$ and $Br^- \cdots CHCl_3$ complexes(23). The $I^- \cdots CHCl_3$ complex was studied by the Caldwell group(51), while $Br^- \cdots CH_3Cl$ was studied by the Li group(52).

1.6 Project Aims

This project has three main aims:

1. Formation of gas-phase van der Waals clusters of halides (Br^- and I^-) with chloromethanes (CH_3Cl, CH_2Cl_2, $CHCl_3$, CCl_4).
2. Study the intermolecular interactions of the previously mentioned van der Waals clusters using MS and PES.
3. Complement the experimental data with high level *ab initio* calculations.

The intermolecular interactions between the halides and chloromethanes will be rationalised in terms of hydrogen and halogen bonding. The computational data will allow the characterisation of the geometries for each complex, as well as other various data which include bond dissociation energies and vibrational mode frequencies. Binding energies obtained from PES can be compared to theoretical calculations to determine the most likely structure of each complex.

Chapter 2

Materials and Methods

The following chapter will outline the experimental and computational techniques used in this project. This includes an explanation of the gas mixture preparation, the various components of the time-of-flight photoelectron spectrometer (TOF-PES), and the spectral data analysis. Furthermore, details of the computational methods and analysis will be covered briefly.

2.1 Experimental Methods

The experimental setup is based on a Wiley-McLaren(53) style mass spectrometer, coupled with a photoelectron spectrometer. The TOF-PES used in this project was constructed in 2008 by LaMacchia and supervised by Wild(54). A diagram of the mass spectrometer is shown in Figure 2.1.

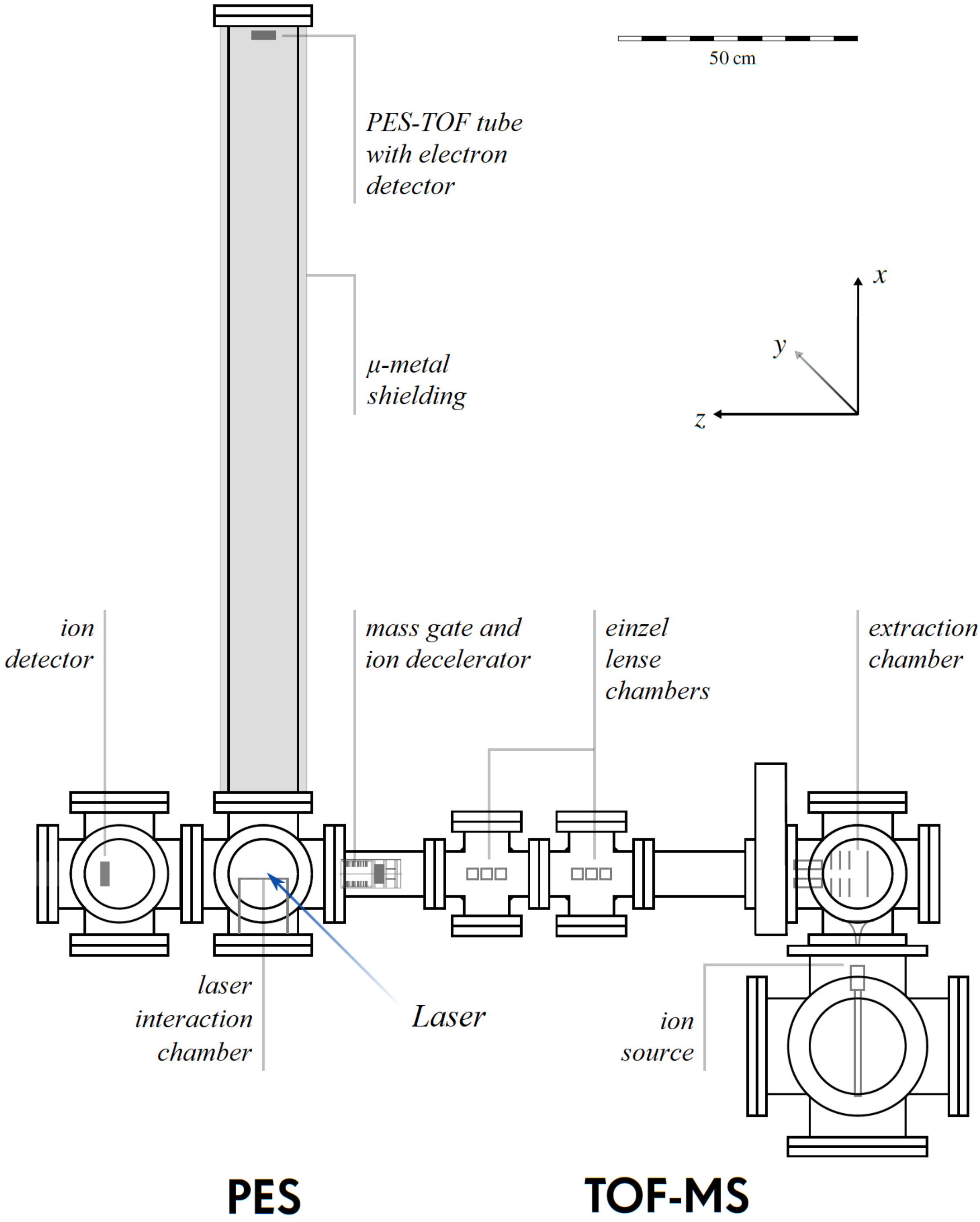

Figure 2.1: Schematic for the mass spectrometer, adapted from Kettner(55).

2.1.1 Gas Mixture Station

In order to form halide chloromethane van der Waals clusters, an appropriate initial gas mixture needs to be prepared. This will consist of argon, the solvating species (chloromethanes), and the halide source (CH_2Br_2 for Br^-, CH_3I for I^-). Argon is used firstly as a carrier gas, and secondly to vibrationally cool down the ion complexes that form.

Before a new gas mixture is prepared, any gases present in the chamber must be evacuated. This is achieved by pumping out the chamber using a rotary pump which is combined with a liquid nitrogen cold trap, and then flushing the chamber with argon. This process is repeated at least three times to ensure that the previous mixture has been properly evacuated and desorbed from the chamber walls. Once the chamber has been evacuated, a small volume of the liquid halide source and solvating species are introduced via two attached vials. The liquid samples are degassed using a freeze-pump-thaw method. This involves freezing the samples with a liquid nitrogen filled dewar, then pumping on the headspace of the vials to vacuum, and finally thawing the samples with a heat gun. This process is repeated three times to ensure the samples are of high purity. The samples are introduced to the gas mixture chamber by way of their vapour pressure, which is achieved by cooling the samples in an ice-water-salt bath, and then opening the headspace of each species to the chamber for about five seconds. Lastly, argon is added to the chamber until the pressure reaches approximately 400 kPa. This process is typically done a day before experiments are run, as the newly created gas mixture requires some time to equilibrate in the chamber.

2.1.2 Ion Source Chamber

The ion source chamber is typically kept at a pressure of about 1×10^{-8} Torr when not in use. When an experiment is being conducted, pressure in the source chamber increases to around 5×10^{-5} Torr, and the gas mixture is injected into the chamber via a pulsed piezo nozzle. This allows the gas to undergo a supersonic expansion when subject to the low pressure. The resulting gas expansion is bombarded by a beam of electrons that are produced from a rhenium filament. A Wehnelt shield positioned behind the filament accelerates the electrons, and an Einzel lens situated in front of the filament allows the electrons to be focussed to a small region in the gas expansion. Additionally, the electron beam can be controlled externally to adjust the current emitted, as well as the pulse timing and width to optimise the conditions of bombardment. When the electrons interact with the gas, a series of dissociative electron attachment reactions take place, which result in the formation of anion complexes as demonstrated in equations 2.1, 2.2 and 2.3.

$$\mathrm{Ar} + e^-_{fast} \longrightarrow \mathrm{Ar}^+ + e^-_{slow} + e^-_{fast} \tag{2.1}$$

$$e^-_{slow} + \mathrm{CH_2Br_2} \longrightarrow [\mathrm{CH_2Br_2}]^{*-} \longrightarrow \mathrm{CH_2Br}^{\bullet} + \mathrm{Br}^- \tag{2.2}$$

$$\mathrm{Br}^- + \mathrm{CCl_4} \longrightarrow \mathrm{Br}^- \cdots \mathrm{CCl_4} \tag{2.3}$$

As well as anion complexes, cations and neutral species are also formed in the gas mixture, resulting in a plasma. A conical skimmer positioned in front of the solenoid nozzle is used to form a collimated plasma beam, where only a small portion of the species present are allowed to enter the extraction chamber. In the extraction chamber, the anion species are separated from the cation and neutral species, before being accelerated down a flight tube.

2.1.3 Extraction Chamber and Flight Tube

A series of TOF plates are used to separate the anion species from the cation and neutral species. This consists of two negatively charged plates, the first set to a voltage of -1500 V, while the second is set to -1350 V. Cations are attracted to the -1500 V plate, while neutral species are unaffected by the plates and collide with the chamber walls. The anion species are initially repelled by the -1500 V plate towards the flight tube, while the -1350 V plate is used to allow space focussing of the anion beam. A third TOF plate is set to ground potential, so that the anion beam experiences field free flight. This is important, because each anion should have approximately the same kinetic energy and thus the individual anions can be separated based solely on their mass over the duration of the flight tube. Anions with a smaller mass will have a higher velocity after being accelerated by the TOF plates, and hence they will arrive at the detector before anions that have a larger mass.

Two sets of X-Y deflection plates are used to help steer the anion beam and correct any deviations in its trajectory. There is one set of plates positioned just before the flight tube, while the other set is positioned midway along the flight tube. The voltage of each individual plate can be varied between -100 V and 100 V, and is adjusted to improve the ion signal at the mass detector or to allow more favourable interactions with the laser. During flight, the individual anions in the beam have a tendency to repel each other. To reduce this effect, the flight tube is lined with a number of Einzel lenses. The Einzel lenses are used to refocus the beam, and similar to the X-Y deflection plates, correct any deviations in its trajectory.

At the end of the flight tube before the laser interaction chamber, there is a mass gate and decelerator unit. The mass gate is used to only allow anions of a specific m/z ratio to enter the interaction chamber. This is achieved through a series of charged plates. The charged plates are set to ground potential for the transit of the desired m/z ratio, whilst held at a high negative voltage to deflect all other anions. The decelerator unit is used to slow the incoming anions for photodetachment. This is important, because it reduces the amount of Doppler broadening in the photoelectron spectrum, and hence improves resolution(56).

2.1.4 Laser Interaction Chamber

To induce photodetachment of electrons, a laser pulse is timed to overlap with the anions of interest. The laser source is a Spectra-Physics Quanta-Ray Pro-230, neodymium doped yttrium aluminium garnet (Nd:YAG) laser that produces a fundamental wavelength of 1064 nm. The frequency of the laser is then quadrupled to produce 266 nm radiation for use in photodetachment. The laser radiation is directed to the interaction chamber where it is used to detach photoelectrons from the desired anions, forming the neutral complex in the process. The laser is pulsed at a rate of 10 Hz.

Once detached, photoelectrons are guided down a 1.6 m photoelectron tube by a permanent magnet which produces a bottleneck-shaped magnetic field when overlapped by a second homogeneous field applied along the length of the photoelectron tube. This setup allows for the capture of as many photoelectrons as possible(56). The photoelectron tube is shielded by a μ-metal which prevents any stray magnetic fields from affecting photoelectrons during their flight. Photoelectrons are recorded at the detector based on their time of flight with respect to the timing of the laser pulse.

In order to accurately determine the time of flight associated with photoelectron detachment, the timing for all components associated with the TOF-PES needs to be controlled. This includes the timing at which gas is injected from the solenoid nozzle, to the timing of a laser pulse. In this project, this is controlled by two pulse generators (SRS, DG535, Four channel digital delay/pulse generator).

2.2 Experimental Data Analysis

The experimental data for photoelectron detachment and for mass spectrometry are all recorded in terms of time of flight. However, these values need to be converted to electron binding energy (eV) and mass to charge (m/z) ratio respectively. The process behind these conversions will be outlined below.

2.2.1 Mass Spectrometry

The time of flight data collected for mass spectrometry is recorded by a digital oscilloscope (Agilent Technologies, DSO6032A, 300 MHz). A spectrum is plotted based on the average of 128 nozzle pulses, where one pulse produces one spectrum. Calibrating the spectrum on a computer requires assigning m/z ratios to the time-of-flight data associated with bare halides, distinguishable by their large signal and isotopic ratio ($^{35}\mathrm{Cl}^-$, $^{37}\mathrm{Cl}^-$, $^{79}\mathrm{Br}^-$, $^{81}\mathrm{Br}^-$ and $^{127}\mathrm{I}^-$). Once calibrated, the m/z ratio of unknown peaks can be determined. Before photoelectron spectra are taken, the m/z peak for the desired anion is optimised to give the best possible intensity for PES. For anions containing species with multiple stable isotopes, choosing the largest m/z peak will give the largest intensity. Other methods of improving intensity may include tuning the electron filament voltage to maximise the number of anions formed without overwhelming the photoelectron detector, fine-tuning the X-Y deflection plates for photodetachment, and modifying the position of the permanent magnet to maximise the capture of photoelectrons.

2.2.2 Photoelectron Spectroscopy

When recording a photoelectron spectrum, each individual photoelectron is detected by a microchannel plate detector as one distinct event. Events are assigned alongside a series of 2 ns wide time bins by an ultra-fast analyser (FAST ComTec, P7888). Time bins are converted to time-of-flight as shown in equation 2.4.

$$\mathrm{TOF} = (16(fstchan) + 2(bin - 1)) \times 10^{-9} \tag{2.4}$$

The $fstchan$ term refers to the start delay, and is usually set to zero, while the bin term refers to the time bin number. Once converted, a photoelectron spectrum will be shown as a series of photoelectron counts as a function of time-of-flight. In order to convert from time-of-flight to kinetic energy, calibration spectra of bare halides are taken. The $^2P_{3/2}$ and $^2P_{1/2}$ peaks of halides (usually bromide and iodide) are determined in terms of time-of-flight, and can then be compared to literature kinetic energy values(57-59), as summarised in Table 2.1. This is achieved by plotting the known kinetic energies against $1/\mathrm{TOF}^2$ values, which results in a linear equation as shown in equation 2.5.

$$e_{\mathrm{KE}} = m\left(\frac{1}{\mathrm{TOF}^2}\right) + c \tag{2.5}$$

From equation 2.5, the values of m and c can be determined through a linear regression analysis. These values can then be used to convert the remaining photoelectron spectra in terms of electron kinetic energy, which includes any spectra of the target anions, as well as background spectra. Lastly, in order to convert to electron binding

Table 2.1: Literature kinetic energies of photoelectrons detached from halides using a 266 nm laser.

Halide	Peak	Literature e_{BE} (eV)	e_{KE} at 266 nm (eV)
Br^-	$^2P_{3/2}$	3.364	1.297
	$^2P_{1/2}$	3.820	0.841
I^-	$^2P_{3/2}$	3.059	1.602
	$^2P_{1/2}$	4.002	0.659

energy, the kinetic energies are subtracted from the energy of the laser (4.661 eV), as described by equation 1.6 in the previous chapter.

Photoelectron spectra are usually recorded over 10,000 laser shots. When recording spectra of the anion of interest, experiments alternate between recording photoelectron spectra and recording background spectra. This is performed multiple times, where each photoelectron spectrum is added together to build up the peaks, and the background for each spectrum is subtracted to give an average spectrum. After applying the necessary conversions so that the spectra are expressed in terms of electron binding energy, a Jacobi transform is required. This involves multiplying the intensities by a factor of TOF^3, and is required because the conversion from time-of-flight to electron kinetic energy is non-linear. The final photoelectron spectrum is therefore a plot of the Jacobi-transformed intensities as a function of electron binding energy over the range of 0 to 4.661 eV.

2.3 Computational Methods

The computational calculations were performed using a combination of Gaussian09(60) and CFOUR(61). Dunning's augmented, correlation consistent, polarised valence X zeta basis sets(36,62-65) were used for all *ab initio* calculations in this project. They take on the general form of:

aug-cc-pVXZ, where X = D, T, Q, 5

Dunning's aug-cc-pVXZ basis sets were applied to carbon and hydrogen atoms in each system. Diffuse functions were applied to chlorine atoms with the aug-cc-pV(X+d)Z basis sets, while pseudopotentials were applied to bromide and iodide atoms with the aug-cc-pVXZ-PP basis sets. These custom basis sets were downloaded from Basis Set Exchange(66). From this point forward, Dunning's basis sets and any of its derivatives will all be referred to as the AVXZ basis sets.

The AVXZ basis sets were an attractive choice for this project because they take into account valence-valence electron contributions, and by definition already include polarisation functions. The term 'augmented' represents the addition of diffuse functions (not to be confused with the 'X+d' diffuse functions on chlorine), while 'correlation consistent' refers to the Gaussian functions that account for electron correlation. One advantage of these basis sets is that they have convergence properties, which makes them highly accurate. Basis set extrapolation methods were therefore able to be used to estimate the complete basis set (CBS) limit, which will be detailed in section 2.4.

Geometry optimisation calculations are performed in this project, and are useful in visualising the structure of the different complexes formed, and how bond lengths and angles vary depending on whether the halide is hydrogen or halogen bonding to the chloromethane. Vibrational frequency calculations are performed to verify whether the optimised geometry is a minimum on the potential energy surface. If there is an imaginary frequency, then the optimised geometry is a transition structure. If all frequency modes are real, then the optimised structure is a true minimum. Single point energy calculations are performed to save time and reduce the computational cost of calculations involving large basis sets. These are also performed in this project to determine the VDE of each anion complex without having to optimise the neutral structure.

Preliminary calculations were run at MP2/AVDZ level of theory to test each possible isomer that could exist. Once the minima were established, geometry optimisations were performed at MP2/AVQZ. Vibrational frequency modes were calculated at MP2/AVQZ, while single point energies were scaled up to MP2/AV5Z in order to perform a CBS extrapolation. From MP2/AVQZ geometries, CCSD(T) single point energies were calculated using AVDZ, AVTZ and AVQZ basis sets, to perform a CBS extrapolation once again. Similarly, CCSD(T)/AVTZ geometry optimisations were run on a select number of systems that were feasible within the time restraints of honours.

Lastly, the M06-2X functional(67) is used, performing geometry optimisations at M06-2X/6-31+G(d,p)(68,69) and upscaling single point energies up to M06-2X/6-311++G(3df,3pd)(70,71) level of theory. The motivation behind this set of calculations is that one study by the Zhang group performed these specific density functional theory (DFT) calculations on $Br^- \cdots (CCl_3Br)_{0-2}$ complexes, and claimed that the "M06-2X functional is widely accepted to describe halogen bonding" in the supplementary information of the journal article(72). As the aforementioned study has similarities with this project, obtaining a dataset with M06-2X and comparing it with the MP2 and CCSD(T) datasets adds a new layer to the results and discussion of this project.

2.4 Computational Data Analysis

When running a calculation, energy values are output as a unit of Hartree. While energy values of Hartree can be compared with each other, this can only be achieved when the energy values were calculated using the same level of theory and basis set. To compare across different datasets, a standardised unit of measurement is required. Dissociation energies measure the amount of energy required to form or break a chemical bond, and are an indicator of the strength of an interaction. For van der Waals complexes, this will be a measure of how much energy is required to form the complex from the individual substituents, with an example shown in equation 2.6. The energy difference between the individual substituents and the complex is multiplied by 2625.5 kJ mol^{-1} Hartree^{-1} to give a dissociation energy represented in kJ mol^{-1}. Dissociation energies can then be compared across different datasets.

$$E(\mathrm{Br}^-) + E(\mathrm{CCl_4}) \longrightarrow E(\mathrm{Br}^- \cdots \mathrm{CCl_4}) \tag{2.6}$$

Calculation of vertical detachment energies requires a number of steps before it can be compared to experimental peaks. Firstly, a single point energy calculation of a neutral complex needs to be run from the optimised anion geometry (i.e. the charge is decreased by one, and multiplicity increases). The VDE is then calculated in eV as demonstrated in equation 2.7, using the conversion factor 27.211 eV Hartree^{-1}. The corrected zero-point energy (zpe) is a term that is subtracted so that the VDE is calculated from the vibrational ground state $\nu'' = 0$, as shown previously in Figure 1.1. The corrected zpe only takes into account the vibrational modes ω that involve both the halide and the neutral molecule, which for the halide chloromethane complexes was always based on the three smallest modes (ω_n, ω_{n-1} and ω_{n-2}), with

ω_1 being defined as the largest mode (in cm^{-1}). It is calculated as shown in equation 2.8 using the conversion factor $1.2398{\times}10^{-4}$ eV cm.

$$\mathrm{VDE} = 27.211\left(\left|E(\mathrm{X}^{-}\cdots\mathrm{A})\ - E(\mathrm{X}\cdot\cdots\mathrm{A})\right|\right) - \text{Corrected zpe} \tag{2.7}$$

$$\text{Corrected zpe} = 1.2398{\times}10^{-4}\left(\frac{\omega_n + \omega_{n-1} + \omega_{n-2}}{2}\right) \tag{2.8}$$

At this point, the calculated VDE is only a ^2P electronic state. A term known as the spin-orbit constant is required in order to determine the theoretical spin-orbit splitting. The spin-orbit constant measures the point at which two electronic states diverge based on the difference in their total angular momentum quantum number j. The spin-orbit splitting values that arise are essentially energy values relative to the calculated VDE, and are shown below in Table 2.2.

Table 2.2: Calculation of spin-orbit splitting of bromide and iodide.

	SO Split*	SO Constant	$^2P_{3/2}$ Split		$^2P_{1/2}$ Split	
	(cm^{-1})	(cm^{-1})	(cm^{-1})	(eV)	(cm^{-1})	(eV)
Br^-	3685.24	-2456.83	-1228.41	-0.152	2456.83	0.305
I^-	7603.15	-5068.77	-2534.38	-0.314	5068.77	0.628

*Values based on experiment(59)

For bromide, the splitting is -0.152 eV and +0.305 eV, and for iodide it is -0.314 eV and +0.628 eV, resulting in split $^2P_{3/2}$ and $^2P_{1/2}$ peaks. The split $^2P_{3/2}$ peak is subtracted from the literature $^2P_{3/2}$ electron binding energy value (3.364 eV for bromide, 3.059 eV for iodide)(57,58) to give an energy shift constant, which is applied to each calculated split peak to give a more accurate prediction of the VDE peaks that will be observed in experiment. This shift constant is dependent on the level of theory and basis set.

Basis set extrapolation methods are useful in estimating additional energy contributions in a single point energy calculation, without the need to run optimisation and frequency analysis calculations using larger basis sets. This has the benefit of saving computational time, while still computing accurate results. To estimate the CBS limit, the Hartree-Fock energy (E_{HF}) and the correlation energy (E_{corr}) terms are all extrapolated separately. Equation 2.9 is used for the E_{HF} extrapolation of the MP2 calculations(73), while equation 2.10 is used for the E_{HF} extrapolation of CCSD(T) calculations.

$$E_{HF}^{\infty} = E_{HF}^{L} + \frac{E_{HF}^{L} - E_{HF}^{L-1}}{\frac{L(\exp(9(\sqrt{L}-\sqrt{L-1})))}{L+1} - 1} \tag{2.9}$$

$$E_{HF}^{\infty} = E_{HF}^{L} + \frac{E_{HF}^{L} - E_{HF}^{L-1}}{\left(\frac{L}{L-1}\right)^{\alpha} - 1} \tag{2.10}$$

The value of L refers to the cardinal number of the basis set. For example, a CBS extrapolation from MP2/AVQZ and MP2/AV5Z energies will have cardinal numbers of $L = 4$ and $L = 5$ respectively. In equation 2.10, the α term is set to 5 in accordance with the W1w protocol(74). Equation 2.11 is used for the extrapolation of correlation energy terms, and is almost identical to equation 2.10.

$$E_{corr}^{\infty} = E_{corr}^{L} + \frac{E_{corr}^{L} - E_{corr}^{L-1}}{\left(\frac{L}{L-1}\right)^{\beta} - 1} \tag{2.11}$$

For extrapolation of MP2 energies, the β term is set to 3, as found by Helgaker et al.(75), while for extrapolation of CCSD and (T) energies, the β term is set to 3.22 in accordance with the W1w protocol. HF and CCSD contributions are extrapolated from the AVQZ and AVTZ basis sets, whereas (T) contributions are extrapolated from AVTZ and AVDZ basis sets. Once each of the energy terms has been extrapolated accordingly, the terms are summed back together to give an estimated CBS limit, as shown in equation 2.12.

$$E_{total}^{\infty} = E_{HF}^{\infty} + E_{corr}^{\infty} \tag{2.12}$$

Once the CBS limit has been deduced, dissociation energies and vertical detachment energies are calculated to compare to experimental results and between the different levels of theory.

Chapter 3

Results and Discussion

The following chapter will cover all the experimental and computational results that were obtained in this project. These results include mass spectra recorded from each halide chloromethane gas mixture, photoelectron spectra of $Br^- \cdots CH_2Cl_2$, $Br^- \cdots CHCl_3$ and $Br^- \cdots CCl_4$ accompanied by experimental binding energies, and all geometries and energies calculated computationally. Additionally, the experimental results and computational results will be compared and rationalised in terms of hydrogen and halogen bonding.

3.1 Experimental Results

3.1.1 Mass Spectrometry

Figure 3.1 is the resulting mass spectrum from a gas mixture of dibromomethane, dichloromethane, and argon. The $^{79}Br^-$ and $^{81}Br^-$ peaks can be found at 78.9 m/z and 80.9 m/z respectively, while the $^{127}I^-$ peak can be found at 126.9 m/z. These three halide peaks were used to calibrate the spectrum. The location of the

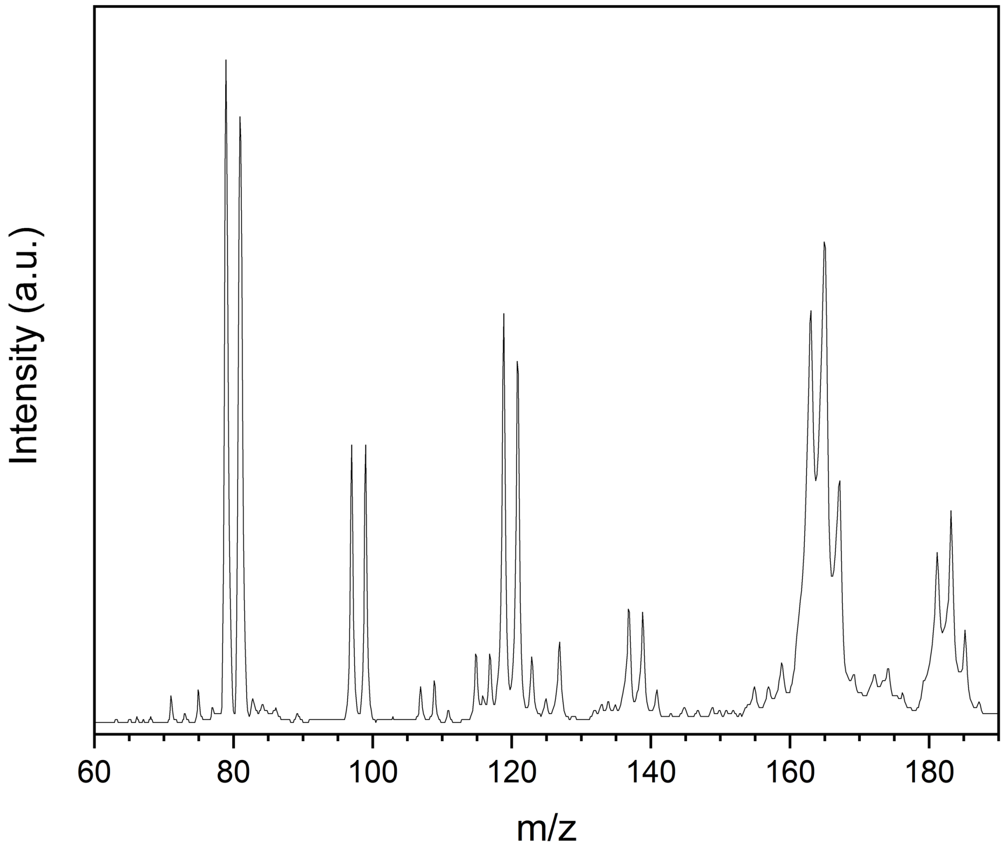

Figure 3.1: Mass spectrum from a gas mixture of CH_2Br_2, CH_2Cl_2 and Ar.

$Br^- \cdots CH_2Cl_2$ species were identified as the second most intense cluster of peaks at 162.9, 164.9, 166.9 and 168.9 m/z, with the number and intensity of the peaks being characteristic of the isotope abundances of ^{79}Br, ^{81}Br, ^{35}Cl, and ^{37}Cl. The two peaks at 118.9 and 120.9 m/z arise as a result of the $Br^- \cdots Ar$ complex, and are almost as intense as the $Br^- \cdots CH_2Cl_2$ peaks, while the $Br^- \cdots H_2O$ complex can be found at 96.9 and 98.9 m/z. Other peaks arise as a result of argon and water complexes, which include the $Br^- \cdots (H_2O)_2$ dimer complex at 114.9 and 116.9 m/z, the $^{79}Br^- \cdots (Ar)_2$ dimer complex at 158.9 m/z, the $Br^- \cdots Ar{\cdot}H_2O$ complex at 136.9 and 138.9 m/z, and the $Br^- \cdots Ar{\cdot}(H_2O)_2$ complex at 154.9 and 156.9 m/z. Interestingly, the $Br^- \cdots CH_2Cl_2{\cdot}H_2O$ complex is found as a series of peaks between 180.9 and 186.9 m/z, and the bromide-bromomethyl radical complex that was recently studied by the Wild group(76) can be observed at 171.9, 173.9

and 175.9 m/z. The $\text{Cl}^- \cdots \text{CH}_2\text{Cl}_2$ complex can be identified as a series of peaks at 118.9, 120.9, 122.9 and 124.9 m/z, however the 118.9 and 120.9 m/z peaks overlap with the $\text{Br}^- \cdots \text{Ar}$ complex.

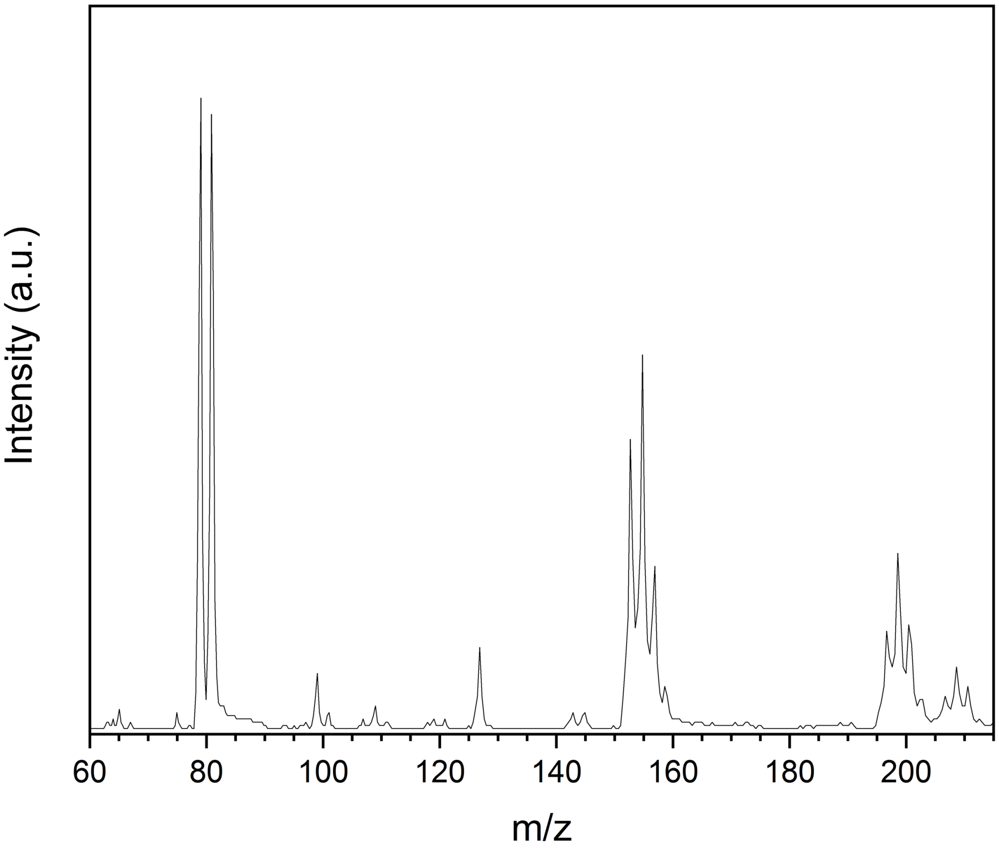

Figure 3.2: Mass spectrum from a gas mixture of CH_2Br_2, CHCl_3 and Ar.

A gas mixture of dibromomethane, trichloromethane and argon resulted in the mass spectrum that is presented in Figure 3.2. The $^{79}\text{Br}^-$ and $^{81}\text{Br}^-$ peaks at 78.9 m/z and 80.9 m/z respectively, as well as the $^{127}\text{I}^-$ peak at 126.9 m/z were used to calibrate the mass spectrum. The two bromide peaks are the most intense, followed by the $\text{Cl}^- \cdots \text{CHCl}_3$ complex at 152.9, 154.9, 156.9 and 158.9 m/z, and then the $\text{Br}^- \cdots \text{CHCl}_3$ complex at 196.8, 198.8, 200.8 and 202.8 m/z. The four peaks at 205.8, 207.8, 209.8 and 211.8 m/z arise from the $\text{Cl}^- \cdots \text{CH}_2\text{Br}_2$ complex, while the pair of peaks at 74.9 and 76.9 m/z, and the pair of peaks at 118.9 and 120.9 m/z are observed due to the $\text{Cl}^- \cdots \text{Ar}$ and $\text{Br}^- \cdots \text{Ar}$ complexes respectively. These two argon complexes are of very low intensity compared to the bare bromide peaks. Lastly, two pairs of peaks arise due to the complexes $Cl^- \cdots SO_2$ and $Br^- \cdots SO_2$, which are found at 98.9, 100.9, 142.9 and 144.9 m/z. These complexes are formed due to residue gas that had desorbed from the walls within the gas mixing station from previous experiments.

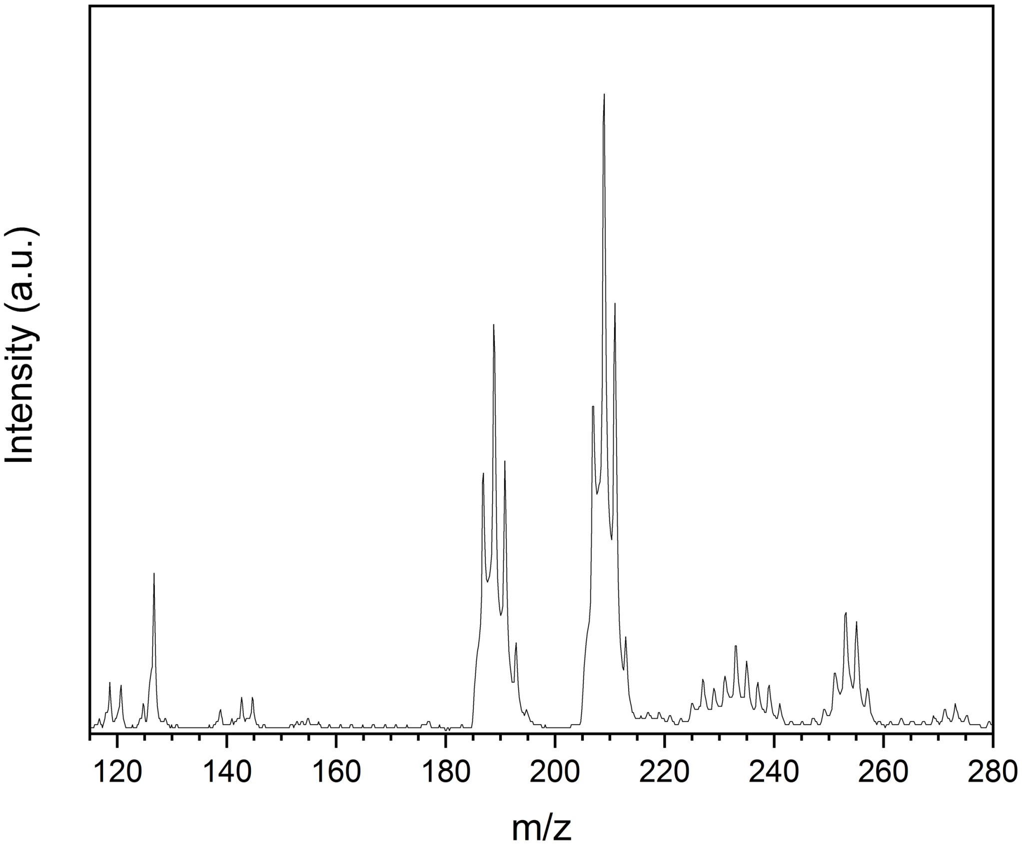

Figure 3.3: Mass spectrum from a gas mixture of CH_2Br_2, CCl_4 and Ar.

The mass spectrum shown in Figure 3.3 was recorded from a gas mixture of dibromomethane, tetrachloromethane and argon. The $Cl^- \cdots CCl_4$ complex is observed as a series of peaks at 186.8, 188.8, 190.8, 192.8 and 194.8 m/z, whereas the $Cl^- \cdots CH_2Br_2$ complex is observed at 206.8, 208.8, 210.8 and 212.8 m/z. The $Br^- \cdots CH_2Br_2$ complex can be found as a series of peaks at 250.8, 252.8, 254.8 and 256.8 m/z, while the $Br^- \cdots CCl_4$ complex can be found in a cluster of nine peaks. This cluster of peaks contains two different complexes, with the first three peaks at 224.8, 226.8 and 228.8 m/z corresponding to the $Cl^- \cdots CH_2Br_2{\cdot}H_2O$ complex, and the last five peaks at 232.8, 234.8, 236.8, 238.8 and 240.8 m/z corresponding to the $Br^- \cdots CCl_4$ complex. The peak at 230.8 m/z arises due to an overlap between the $^{37}Cl^- \cdots CH_2(^{81}Br)_2{\cdot}H_2O$ and the $^{79}Br^- \cdots C(^{35}Cl)_4$ complexes. Four peaks of low intensity can be observed at 268.8, 270.8, 272.8 and 274.8 m/z, and these arise from the $Br^- \cdots CH_2Br_2{\cdot}H_2O$ complex. The pair of peaks at 118.9 and 120.9 m/z are a result of the $Br^- \cdots Ar$ complex, while the two peaks at 142.9 and 144.9 m/z correspond to $Br^- \cdots SO_2$, formed from residual SO_2 from a previous experiment.

3.1.2 Photoelectron Spectroscopy

Photoelectron spectra of the $Br^- \cdots CH_2Cl_2$, $Br^- \cdots CHCl_3$ and $Br^- \cdots CCl_4$ complexes are presented here. A summary of experimental binding energies of bare bromide and each complex, as well as E_{stab} values are shown below in Table 3.1. The value of E_{stab} refers to the stabilisation energy, where values greater than zero indicating that the chloromethane molecule coordinating with the halide has provided a stabilising effect to the system. Experimentally, E_{stab} is calculated as the difference in binding energy between the bare halide and the complex, whereas computationally it is calculated as the difference in dissociation energy between the anion and neutral geometries of the complex. E_{stab} can be calculated for both the $^2P_{3/2}$ and $^2P_{1/2}$ electronic states, and should be similar since the spin-orbit splitting pattern does not change appreciably when a halide forms a complex.

The photoelectron spectrum presented in Figure 3.4 is the average of two individual spectra of the $Br^- \cdots CH_2Cl_2$ complex recorded on the same day. The most intense peak at 3.98 eV corresponds to the $^2P_{3/2}$ peak, whereas the $^2P_{1/2}$ peak is at 4.44

Table 3.1: Experimentally determined binding energies of bromide chloromethane complexes, in eV.

	Br^-		Complex		E_{stab}	
	$^2P_{3/2}$	$^2P_{1/2}$	$^2P_{3/2}$	$^2P_{1/2}$	$^2P_{3/2}$	$^2P_{1/2}$
$Br^- \cdots CH_2Cl_2$	3.36	3.82	3.98	4.44	0.62	0.62
$Br^- \cdots CHCl_3$	3.36	3.82	4.09	4.51	0.73	0.69
$Br^- \cdots CCl_4$	3.36	3.83	3.85	4.29	0.49	0.46

eV. The E_{stab} value of the $Br^- \cdots CH_2Cl_2$ complex is 0.62 eV for the $^2P_{3/2}$ peak, and 0.62 eV for the $^2P_{1/2}$ peak, positive values indicating that the halide has been stabilised by the CH_2Cl_2 molecule. Similarly, no change between the E_{stab} values for the $^2P_{3/2}$ and $^2P_{1/2}$ electronic states implies that the CH_2Cl_2 molecule has not affected the spin-orbit splitting of bromide.

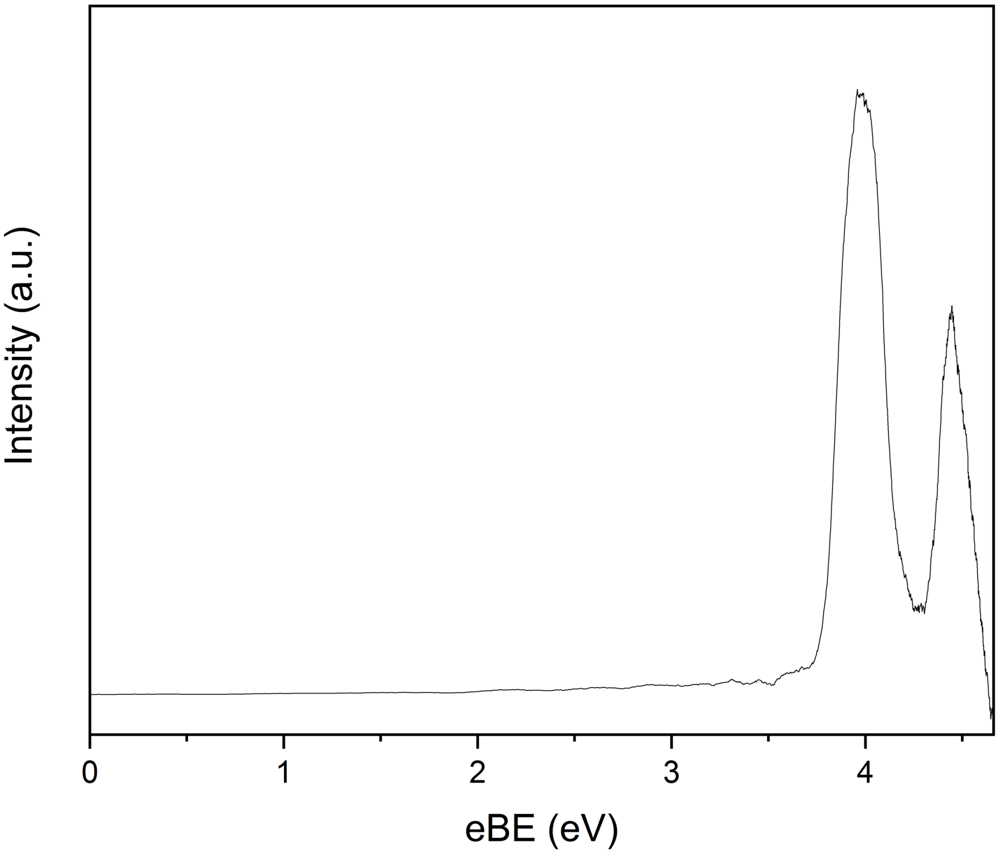

Figure 3.4: Photoelectron spectrum of the $Br^- \cdots CH_2Cl_2$ complex.

Figure 3.5 displays the average of four individual photoelectron spectra of the $Br^- \cdots CHCl_3$ complex recorded on the same day. The two peaks at 4.09 eV and

4.51 eV correspond to the ${}^2P_{3/2}$ and ${}^2P_{1/2}$ electronic states respectively, with E_{stab} values of 0.73 eV for the ${}^2P_{3/2}$ peak and 0.69 eV for the ${}^2P_{1/2}$ peak. The two E_{stab} values differ by 0.04 eV, which may signify a small change in the bromide spin-orbit splitting when interacting with $CHCl_3$. Both E_{stab} values of $Br^- \cdots CHCl_3$ are larger than the E_{stab} values of the $Br^- \cdots CH_2Cl_2$ complex, which indicates that the intermolecular interaction arising in the $Br^- \cdots CHCl_3$ complex is stronger and has an improved stabilising effect on the bromide.

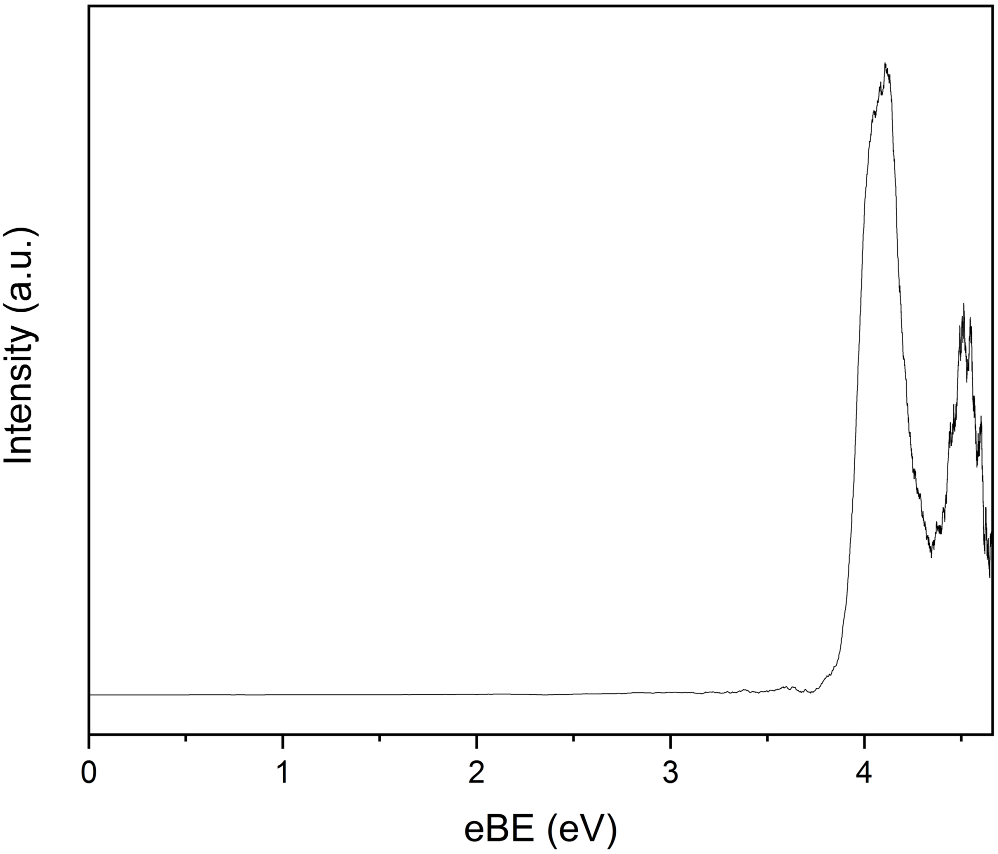

Figure 3.5: Photoelectron spectrum of the $Br^- \cdots CHCl_3$ complex.

The photoelectron spectrum shown in Figure 3.6 is the average of ten individual spectra of the $Br^- \cdots CCl_4$ complex recorded on the same day, where the ${}^2P_{3/2}$ and ${}^2P_{1/2}$ peaks are found at 3.85 eV, and 4.29 eV respectively. The E_{stab} values associated with the two peaks are 0.49 eV and 0.46 eV, differing by 0.03 eV which may be indicative that the CCl_4 molecule affects the spin-orbit splitting of bromide.

Compared to the $Br^- \cdots CH_2Cl_2$ and $Br^- \cdots CHCl_3$ complexes, the stabilisation energy of the $Br^- \cdots CCl_4$ complex is smaller, but positive, which implies that the stabilisation effect of the tetrachloromethane on the bromide is the weakest of the three complexes.

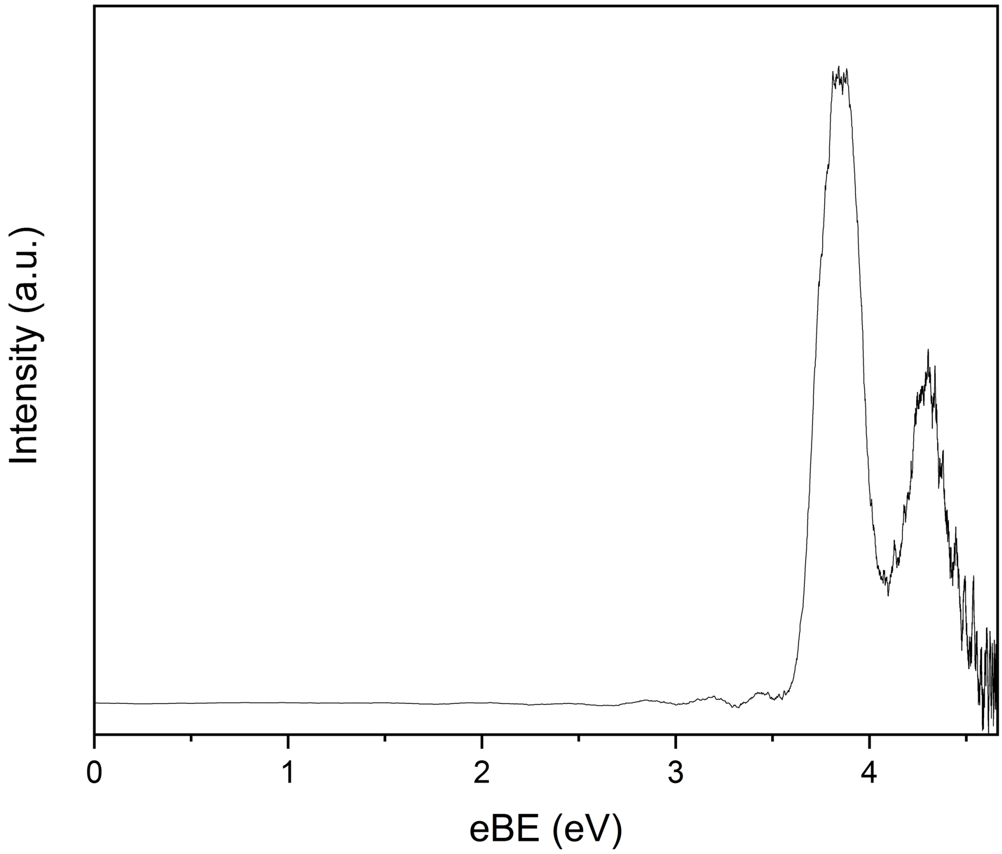

Figure 3.6: Photoelectron spectrum of the $Br^- \cdots CCl_4$ complex.

The experimental results discussed above will be rationalised in subsection 3.2.6 when compared to computational results. However, photoelectron spectra were only recorded for three of the five systems that are studied in this project, so the two remaining systems can only be discussed in terms of theoretical data. The $I^- \cdots CCl_4$ complex will be the top priority for future work in regard to experimental data, while the $Br^- \cdots CH_3Cl$ complex will require obtaining a source of CH_3Cl before photoelectron spectra can be recorded.

3.2 Computational Results

This section will outline the computational results obtained in this project. Each of the four chloromethanes (CH_3Cl, CH_2Cl_2, $CHCl_3$ and CCl_4) and their respective halide complexes are separated into their own subsections. Subsection 3.2.5 will detail the deviations in structural parameters of the complexes relative to the bare chloromethanes, as well as at each level of theory. Calculated dissociation energies and vertical detachment energies are discussed in subsection 3.2.6, and will be used to compare how well each level of theory performs relative to CCSD(T).

3.2.1 Bromide Monochloromethane Complexes

Two structures were found for $Br^- \cdots CH_3Cl$, of which both structures were optimised at M06-2X/6-31+G(d,p), MP2/AVQZ and CCSD(T)/AVTZ. The first structure is of C_{3v} symmetry, which involves the bromide appended to the chlorine atom

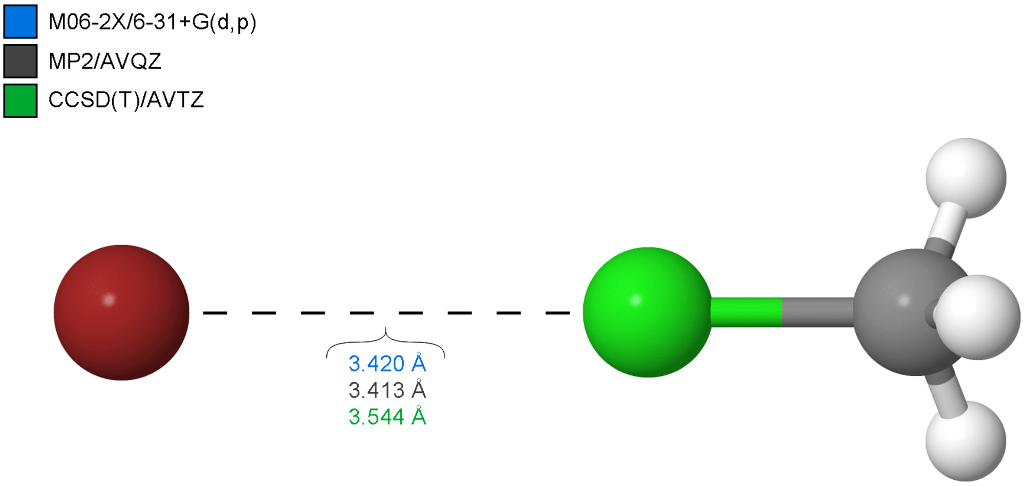

Figure 3.7: Structure of $Br^- \cdots CH_3Cl$ interacting via a halogen bond, optimised at CCSD(T)/AVTZ.

in a halogen bond (XB) motif, shown in Figure 3.7. At CCSD(T), the bromide can be found at a distance of 3.544 Å from the chlorine, whereas this bond length decreases to 3.412 Å and 3.420 Å at MP2 and M06-2X respectively. The bond length between the chlorine and the carbon was found to be 1.784 Å at M06-2X, and 1.783 Å at CCSD(T). At MP2, the C-Cl bond length decreased to 1.769 Å. The C-H bond lengths varied between 1.085 and 1.091 Å.

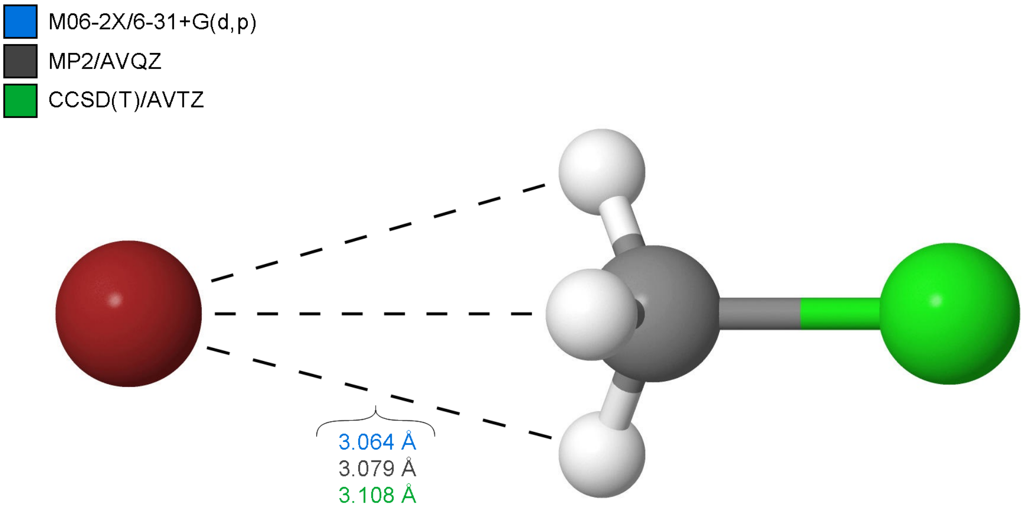

Figure 3.8: Structure of $Br^- \cdots CH_3Cl$ interacting via an ion dipole interaction, optimised at CCSD(T)/AVTZ.

The second structure calculated was also of C_{3v} symmetry, and involves the bromide interacting equidistant to the three hydrogen atoms via an ion dipole (ID) (Figure 3.8). The bromide to hydrogen bond lengths were found to be 3.108 Å at CCSD(T), but decreased to 3.079 Å and 3.064 Å at MP2 and M06-2X levels of theory respectively. The three hydrogen atoms bond at a distance that varied between 1.080 and 1.085 Å to the carbon atom, slightly less than the C-H distance calculated for the halogen bonded complex. The bonding angle the bromide forms with the carbon and hydrogen atoms was calculated to be 71.5° at M06-2X, 71.4° at MP2, and 71.7° at

CCSD(T). A summary of the structural parameters of each $\text{Br}^- \cdots \text{CH}_3\text{Cl}$ complex can be found below in Table 3.2.

Table 3.2: Structural parameters of bromide monochloromethane anion complexes optimised at M06-2X/6-31+G(d,p), MP2/AVQZ and CCSD(T)/AVTZ.

		Theory	$r_{\text{Br}^-\cdots\text{H}}$ Å	$r_{\text{Br}^-\cdots\text{Cl}}$ Å	$r_{\text{C-Cl}}$ Å	$r_{\text{C-H}}$ Å	$\angle_{\text{Br}^-\text{-C-H}}$ °	$\angle_{\text{Br}^-\text{-Cl-C}}$ °
ID	C_{3v}	M06-2X	3.064	5.056	1.826	1.085	71.5	-
		MP2	3.079	5.053	1.805	1.080	71.4	-
		CCSD(T)	3.108	5.095	1.823	1.083	71.7	-
XB	C_{3v}	M06-2X	5.663	3.420	1.784	1.091	-	180.0
		MP2	5.636	3.413	1.769	1.085	-	180.0
		CCSD(T)	5.776	3.544	1.783	1.089	-	180.0

3.2.2 Bromide Dichloromethane Complexes

There were two structures found for the $\text{Br}^- \cdots \text{CH}_2\text{Cl}_2$ system that were optimised at M06-2X/6-31+G(d,p), MP2/AVQZ and CCSD(T)/AVTZ, with both found to be of C_s symmetry. The first structure (Figure 3.9) involves the bromide tethered to one of the hydrogen atoms, by way of a hydrogen bond (HB) interaction. The bond

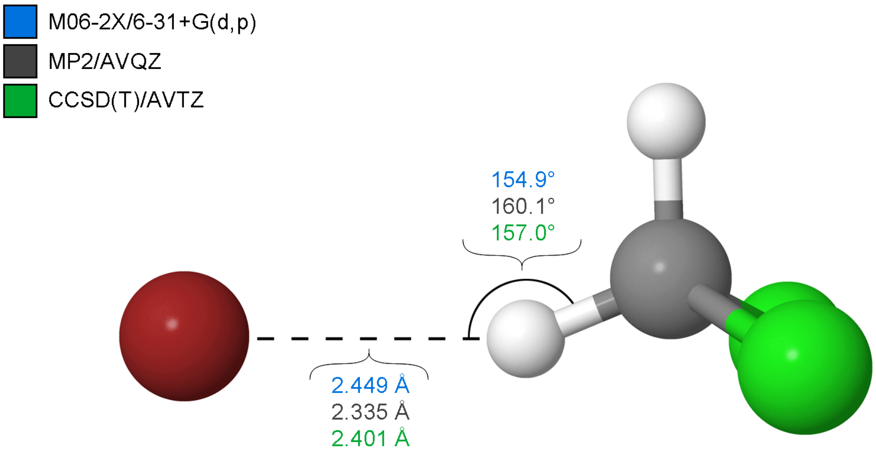

Figure 3.9: Structure of $\text{Br}^- \cdots \text{CH}_2\text{Cl}_2$ interacting via a hydrogen bond, optimised at CCSD(T)/AVTZ.

angle between the bromide, hydrogen and carbon was calculated to be 154.9° at M06-2X, increasing to 157.0° at CCSD(T), and even further up to 160.1° at MP2. At CCSD(T), the hydrogen bond distance is 2.401 Å, but was found to be shorter in the case of MP2. M06-2X predicts the longest hydrogen bond distance of 2.449 Å. The C-H bond length of the non-interacting hydrogen varied between 1.082 and 1.086 Å, compared to the interacting hydrogen where the C-H bond is longer at 1.095-1.096 Å.

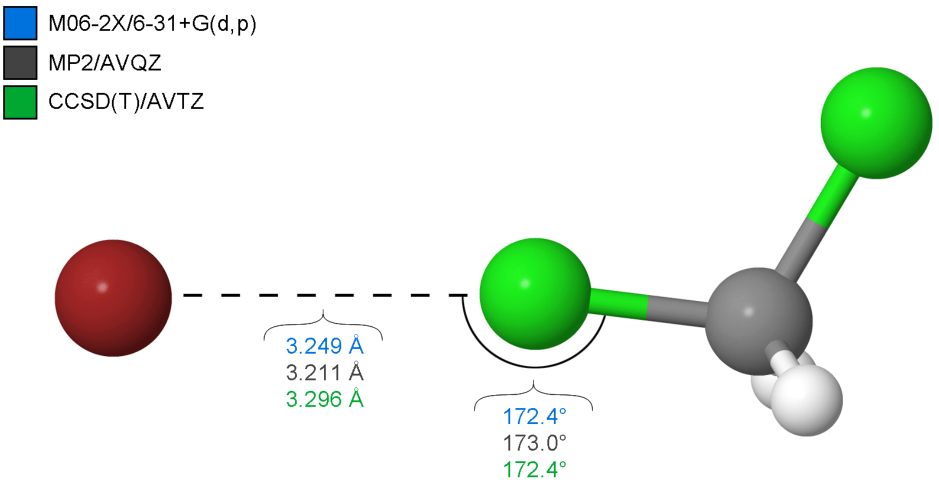

Figure 3.10: Structure of $Br^- \cdots CH_2Cl_2$ interacting via a halogen bond, optimised at CCSD(T)/AVTZ.

The other $Br^- \cdots CH_2Cl_2$ structure involves the bromide interacting with one of the chlorine atoms via a halogen bond, shown in Figure 3.10. The bond angle between the bromide, chlorine and carbon is calculated at both M06-2X and CCSD(T) to be 172.4°, while at MP2 the angle is calculated to be 173.0°. At CCSD(T), the halogen bond length is 3.296 Å. M06-2X and MP2 predict shorter halogen bond lengths of 3.249 Å and 3.211 Å respectively. The C-Cl bond length of the interacting chlorine is 1.748 Å at MP2 theory, but is calculated to be 1.762 Å at CCSD(T), and 1.763 Å at M06-2X. The C-Cl bond length of the non-interacting chlorine was found to be longer than the interacting chlorine, varying between 1.785 Å at MP2 and 1.802 Å at M06-2X. The structural parameters of the two $Br^- \cdots CH_2Cl_2$ complexes can be found below in Table 3.3.

Table 3.3: Structural parameters of the bromide dichloromethane anion complexes optimised at M06-2X/6-31+G(d,p), MP2/AVQZ and CCSD(T)/AVTZ.

		Theory	$r_{\mathrm{Br^-}\cdots\mathrm{H_1}}$ Å	$r_{\mathrm{C-Cl}}$ Å	$r_{\mathrm{C-H_1}}$ Å	$r_{\mathrm{C-H_2}}$ Å	$\angle_{\mathrm{Br^-\text{-}H_1\text{-}C}}$ °
HB	C_s	M06-2X	2.449	1.787	1.095	1.086	154.9
		MP2	2.335	1.771	1.096	1.082	160.1
		CCSD(T)	2.401	1.785	1.095	1.084	157.0
			$r_{\mathrm{Br^-}\cdots\mathrm{Cl_1}}$ Å	$r_{\mathrm{C-Cl_1}}$ Å	$r_{\mathrm{C-Cl_2}}$ Å	$r_{\mathrm{C-H}}$ Å	$\angle_{\mathrm{Br^-\text{-}Cl_1\text{-}C}}$ °
XB	C_s	M06-2X	3.249	1.763	1.802	1.088	172.4
		MP2	3.211	1.748	1.785	1.083	173.0
		CCSD(T)	3.296	1.762	1.799	1.085	172.4

3.2.3 Bromide Trichloromethane Complexes

For the $Br^- \cdots CHCl_3$ system, three structures were located as minima on the potential energy surface. One of the structures involves the bromide appended to the hydrogen atom to form a hydrogen bond interaction (Figure 3.11). This structure is of C_{3v} symmetry, and was optimised at M06-2X/6-31+G(d,p), MP2/AVQZ and CCSD(T)/AVTZ. At CCSD(T), the length of the hydrogen bond was calculated as 2.256 Å. The length of the hydrogen bond is shorter at MP2 and M06-2X, found to be 2.185 Å and 2.234 Å respectively. MP2 predicts a C-H bond length of 1.110 Å, while at CCSD(T) a C-H length of 1.105 Å is found. The length of the C-Cl bond varied between 1.764 Å and 1.779 Å, with the shortest bond length being calculated at MP2, and the longest bond length being calculated at M06-2X.

Another $Br^- \cdots CHCl_3$ structure involves the bromide interacting with one of the chlorine atoms, shown in Figure 3.12. This structure is of C_s symmetry, and was op-

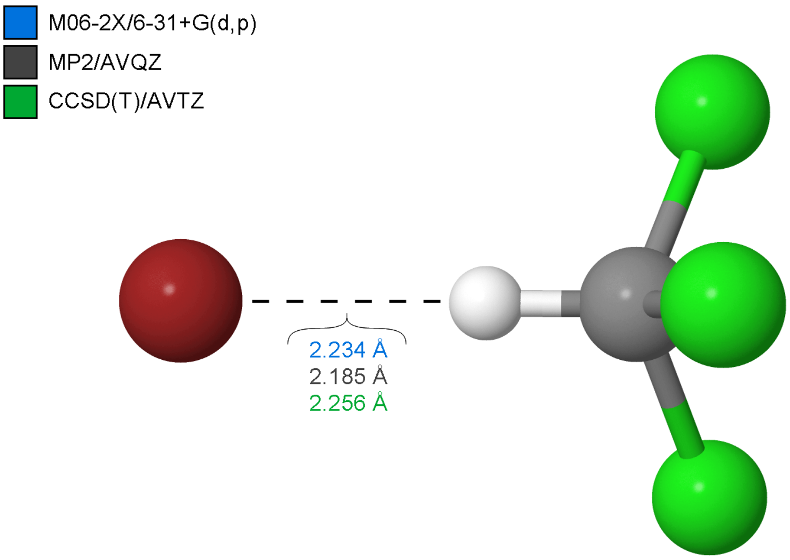

Figure 3.11: Structure of $Br^- \cdots CHCl_3$ interacting via a hydrogen bond, optimised at CCSD(T)/AVTZ.

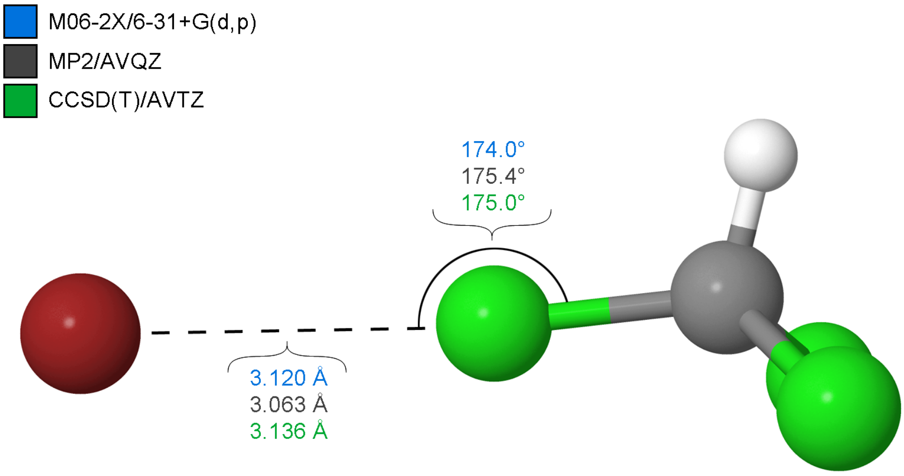

Figure 3.12: Structure of $Br^- \cdots CHCl_3$ interacting via a halogen bond, optimised at CCSD(T)/AVTZ.

timised at M06-2X/6-31+G(d,p), MP2/AVQZ and CCSD(T)/AVTZ. MP2 predicts the shortest halogen bond length at 3.063 Å, which was calculated to be 3.120 Å at M06-2X and 3.136 Å at CCSD(T). The bond angle between the bromide, chlorine and carbon varied between 174.0° and 175.4°. The C-Cl bond length of the interacting chlorine is 1.758 Å at M06-2X, 1.742 Å at MP2 and 1.753 Å at CCSD(T) levels of theory. The C-Cl bond lengths for the two non-interacting chlorine atoms is 1.792 Å at M06-2X, 1.777 Å at MP2 and 1.790 Å at CCSD(T).

The last structure of $Br^- \cdots CHCl_3$ involves the bromide interacting equidistant to the three chlorine atoms, interacting via an ion induced dipole (IID) (Figure 3.13). This structure is of C_{3v} symmetry, and was optimised at M06-2X/6-31+G(d,p) and MP2/AVQZ. In the present work, this structure was not optimised at CCSD(T) due to time constraints.

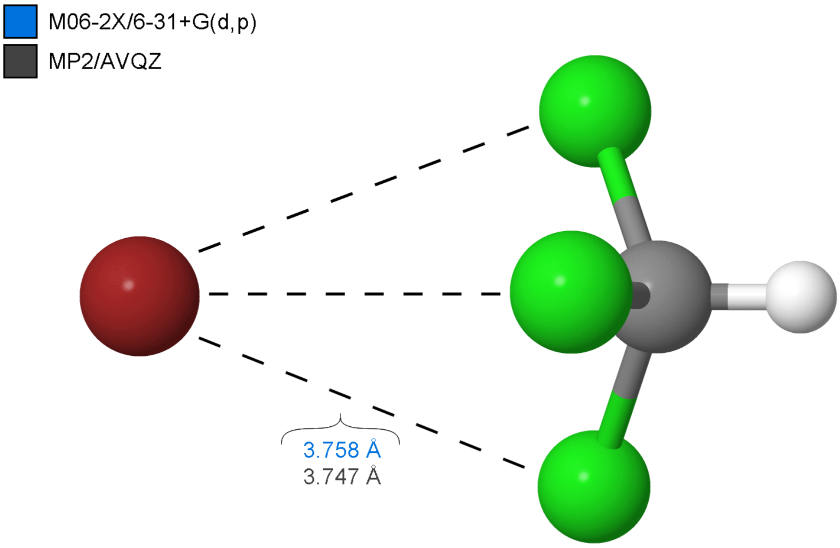

Figure 3.13: Structure of $Br^- \cdots CHCl_3$ interacting via an ion induced dipole, optimised at MP2/AVQZ.

The bromide to chlorine bond length was found to be 3.758 Å at M06-2X, while at MP2 the bond length was found to be shorter at 3.747 Å. The bond angle that the bromide makes with respect to the carbon and chlorine is 73.7° at M06-2X, and 72.7° at MP2. The C-Cl bond length was calculated as 1.755 Å at MP2, and 1.768 Å at M06-2X. At MP2, the C-H bond length is 1.081 Å, whereas at M06-2X the C-H bond length is 1.086 Å. From previous CCSD(T) calculations, bond lengths are typically longer than those found at MP2, so in the case of the $\mathrm{Br}^- \cdots \mathrm{CHCl}_3$ interacting via an ion induced dipole, bond lengths found at CCSD(T) will likely be longer than those reported at MP2. Similarly, from previous results, C-Cl and C-H bond lengths found at M06-2X are not likely to change significantly at CCSD(T), whereas the $\mathrm{Br}^- \cdots \mathrm{Cl}$ bond length could increase relative to M06-2X. Table 3.4 offers a summary of the structural parameters of all three $\mathrm{Br}^- \cdots \mathrm{CHCl}_3$ complexes.

Table 3.4: Structural parameters of the bromide trichloromethane anion complexes optimised at M06-2X/6-31+G(d,p), MP2/AVQZ and CCSD(T)/AVTZ.

		Theory	$r_{\mathrm{Br}^- \cdots \mathrm{H}}$ Å	$r_{\mathrm{Br}^- \cdots \mathrm{Cl}}$ Å	$r_{\mathrm{C-Cl}}$ Å	$r_{\mathrm{C-H}}$ Å	$\angle_{\mathrm{Br}^-\text{-H-C}}$ °	$\angle_{\mathrm{Br}^-\text{-C-Cl}}$ °
HB	C_{3v}	M06-2X	2.234	4.256	1.779	1.109	180.0	-
		MP2	2.185	4.211	1.764	1.110	180.0	-
		CCSD(T)	2.256	4.280	1.777	1.105	180.0	-
IID	C_{3v}	M06-2X	4.934	3.758	1.768	1.086	-	73.7
		MP2	4.955	3.747	1.755	1.081	-	72.7
			$r_{\mathrm{Br}^- \cdots \mathrm{Cl}_1}$ Å	$r_{\mathrm{C-Cl}_1}$ Å	$r_{\mathrm{C-Cl}_2}$ Å	$r_{\mathrm{C-H}}$ Å	$\angle_{\mathrm{Br}^-\text{-Cl}_1\text{-C}}$ °	
XB	C_s	M06-2X	3.120	1.758	1.792	1.086	174.0	
		MP2	3.063	1.742	1.777	1.082	175.4	
		CCSD(T)	3.136	1.753	1.790	1.083	175.0	

3.2.4 Halide Tetrachloromethane Complexes

The bromide tetrachloromethane complexes and the iodide tetrachloromethane complexes each have two structures that were found. The two $\mathrm{Br}^- \cdots \mathrm{CCl}_4$ structures were optimised at M06-2X/6-31+G(d,p) and MP2/AVQZ, whereas the two $\mathrm{I}^- \cdots \mathrm{CCl}_4$ structures were only optimised at MP2/AVQZ due to the 6-31+G(d,p) basis set being insufficient for calculations involving iodine. One structure that was calculated involves the halide appended linearly to one of the chlorine atoms (Figure 3.14 and Figure 3.15).

At MP2 theory, the $\mathrm{Br}^- \cdots \mathrm{Cl}$ distance was found to be 2.928 Å, while at M06-2X this distance was found to be 2.994 Å. The C-Cl bond length of the interacting

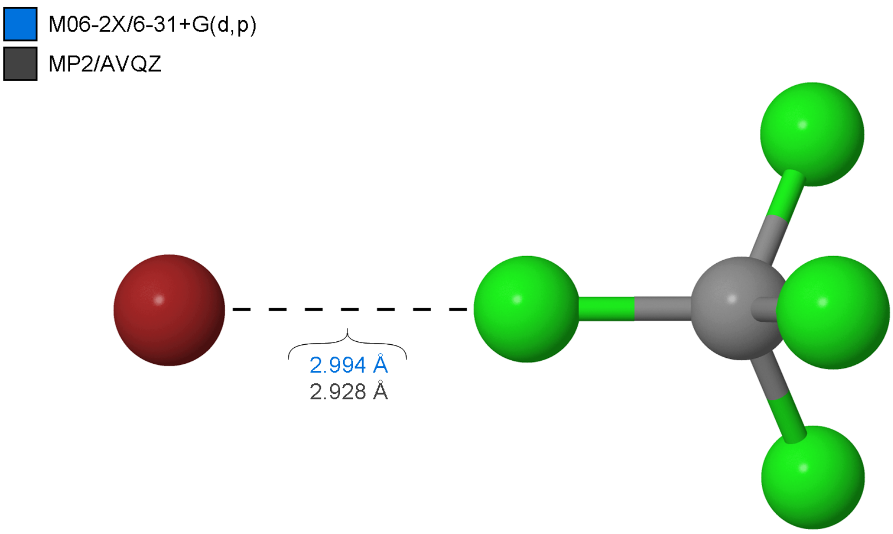

Figure 3.14: Structure of $Br^- \cdots CCl_4$ interacting via a halogen bond, optimised at MP2/AVQZ.

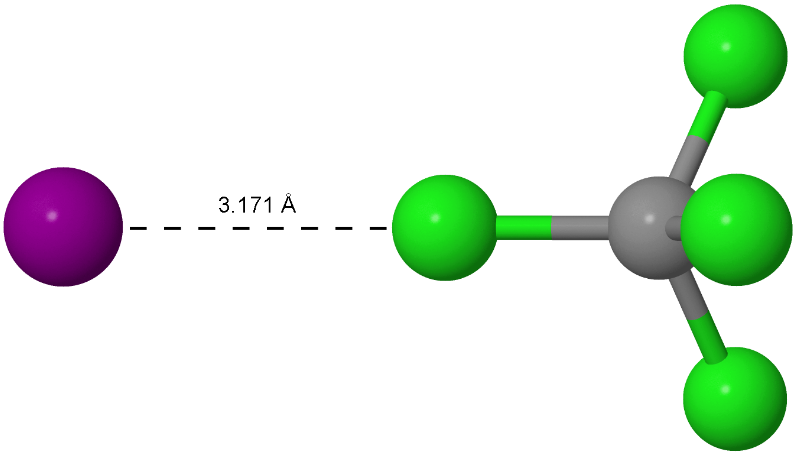

Figure 3.15: Structure of $I^- \cdots CCl_4$ interacting via a halogen bond, optimised at MP2/AVQZ.

chlorine is 1.773 Å at M06-2X, but is found to be 1.753 Å at MP2. The C-Cl bond lengths of the non-interacting chlorine atoms are calculated to be 1.792 Å at M06-2X, and 1.776 Å at MP2. For the halogen bonded $I^- \cdots CCl_4$ complex, the $I^- \cdots Cl$ bond length is 3.171 Å and is longer than the $Br^- \cdots Cl$ bond length. This is indicative of iodide having a larger van der Waals radius than bromide, and will therefore interact at a further distance than bromide. The C-Cl bond length for the interacting chlorine atom is 1.755 Å, shorter than the C-Cl bond length of 1.774 Å for the three non-interacting chlorine atoms.

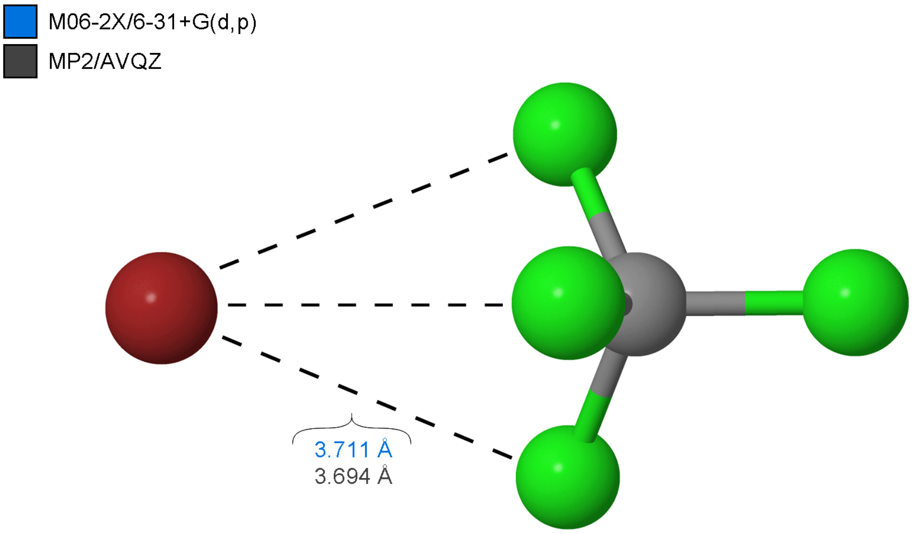

Figure 3.16: Structure of $Br^- \cdots CCl_4$ interacting via an ion induced dipole, optimised at MP2/AVQZ.

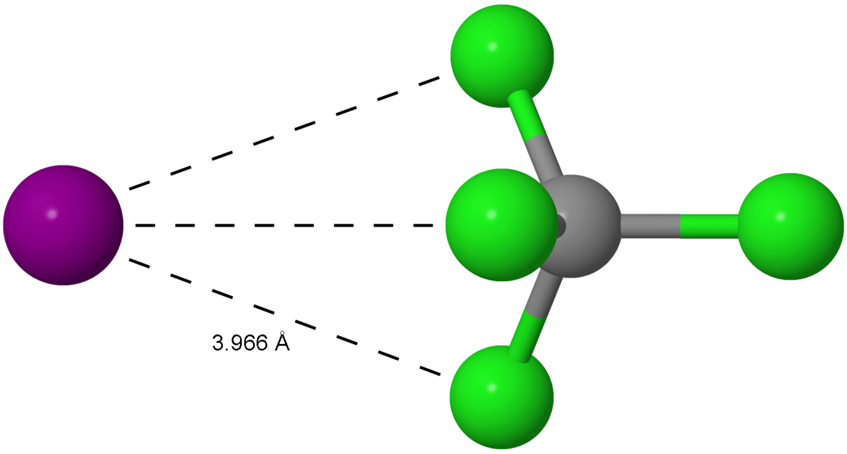

Figure 3.17: Structure of $I^- \cdots CCl_4$ interacting via an ion induced dipole, optimised at MP2/AVQZ.

The second structure calculated for each complex involved the halide interacting equidistant to three chlorine atoms via an ion induced dipole (Figure 3.16 and Figure 3.17). At MP2, the $\text{Br}^- \cdots \text{Cl}$ bond length is 3.694 Å, and at M06-2X the bond length is 3.711 Å. For the iodide complex, the $\text{I}^- \cdots \text{Cl}$ bond length of 3.966 Å is longer than the corresponding $\text{Br}^- \cdots \text{Cl}$ bond length. The bond angle of the halide with respect to the carbon and chlorine was found to be 71.8° at M06-2X, and 71.4° at MP2 for the bromide complex. This angle is found to decrease marginally to 71.3° for the iodide complex. A summary of structural parameters for the two $\text{Br}^- \cdots \text{CCl}_4$ complexes and the two $\text{I}^- \cdots \text{CCl}_4$ complexes can be found below in Table 3.5 and Table 3.6 respectively.

Table 3.5: Structural parameters of the bromide tetrachloromethane anion complexes optimised at M06-2X/6-31+G(d,p) and MP2/AVQZ.

		Theory	$r_{\text{Br}^- \cdots \text{Cl}_1}$ Å	$r_{\text{Br}^- \cdots \text{Cl}_2}$ Å	$r_{\text{C}-\text{Cl}_1}$ Å	$r_{\text{C}-\text{Cl}_2}$ Å	$\angle_{\text{Br}^-\text{-Cl}_1\text{-C}}$ °	$\angle_{\text{Br}^-\text{-C-Cl}_2}$ °
XB	C_{3v}	M06-2X	2.994	5.656	1.773	1.792	180.0	-
		MP2	2.928	5.566	1.753	1.776	180.0	-
IID	C_{3v}	M06-2X	5.674	3.711	1.811	1.764	-	71.8
		MP2	5.649	3.694	1.790	1.750	-	71.4

Table 3.6: Structural parameters of the iodide tetrachloromethane anion complexes optimised at MP2/AVQZ.

		$r_{\text{I}^- \cdots \text{Cl}_1}$ Å	$r_{\text{I}^- \cdots \text{Cl}_2}$ Å	$r_{\text{C}-\text{Cl}_1}$ Å	$r_{\text{C}-\text{Cl}_2}$ Å	$\angle_{\text{I}^-\text{-Cl}_1\text{-C}}$ °	$\angle_{\text{I}^-\text{-C-Cl}_2}$ °
XB	C_{3v}	3.171	5.795	1.755	1.774	180.0	-
IID	C_{3v}	5.953	3.966	1.787	1.751	-	71.3

3.2.5 Comparison of Structural Parameters

The structural parameters of the bare chloromethane molecules are summarised in Table 3.7. At CCSD(T), the hydrogen bonded $\text{Br}^- \cdots \text{CH}_2\text{Cl}_2$ and $\text{Br}^- \cdots \text{CHCl}_3$ complexes had C-H bond lengths that were 0.011 Å and 0.022 Å longer than CH_2Cl_2 and CHCl_3 respectively. Of the three systems where bromide interacts with hydrogen atoms, the ion dipole interacting $\mathrm{Br^- \cdots CH_3Cl}$ complex was the only complex to have a shorter C-H bond length than its respective bare chloromethane, which is a similar outcome to the complexes interacting via ion induced dipoles. While the three C-Cl bond lengths of $\mathrm{Br^- \cdots CHCl_3}$ remain almost unchanged relative to $\mathrm{CHCl_3}$, the $\mathrm{Br^- \cdots CCl_4}$ and $\mathrm{I^- \cdots CCl_4}$ complexes have C-Cl bond lengths that are 0.009 Å and 0.008 Å shorter than $\mathrm{CCl_4}$ respectively.

For the halogen bonded $\mathrm{Br^- \cdots CH_3Cl}$ complex, the C-Cl bond was found to be 0.005 Å shorter relative to $\mathrm{CH_3Cl}$ at CCSD(T). A similar result was found for the halogen bonded $\mathrm{Br^- \cdots CCl_4}$ complex, where at MP2 the C-Cl bond of the interacting chlorine was shorter by 0.006 Å relative to $\mathrm{CCl_4}$, while the C-Cl bond length only decreased by 0.004 Å for the halogen bonded $\mathrm{I^- \cdots CCl_4}$ complex. The C-Cl bond lengths of the halogen bonded $\mathrm{Br^- \cdots CH_2Cl_2}$ and $\mathrm{Br^- \cdots CHCl_3}$ complexes were found to decrease by 0.012 Å and 0.016 Å with respect to $\mathrm{CH_2Cl_2}$ and $\mathrm{CHCl_3}$ at CCSD(T).

Table 3.7: Structural parameters of bare chloromethane molecules optimised at M06-2X/6-31+G(d,p), MP2/AVQZ and CCSD(T)/AVTZ.

		Theory	$r_{\mathrm{C-Cl}}$ Å	$r_{\mathrm{C-H}}$ Å	$\angle_{\text{Cl-C-Cl}}$ °	$\angle_{\text{Cl-C-H}}$ °	$\angle_{\text{H-C-H}}$ °
$\mathrm{CH_3Cl}$	C_{3v}	M06-2X	1.787	1.088	-	108.5	110.4
		MP2	1.773	1.083	-	108.5	110.4
		CCSD(T)	1.788	1.087	-	108.3	110.6
$\mathrm{CH_2Cl_2}$	C_{2v}	M06-2X	1.774	1.086	112.9	108.1	111.5
		MP2	1.760	1.082	112.3	108.3	111.6
		CCSD(T)	1.774	1.084	112.3	108.2	111.9
$\mathrm{CHCl_3}$	C_{3v}	M06-2X	1.771	1.086	111.1	107.8	-
		MP2	1.756	1.082	110.9	108.0	-
		CCSD(T)	1.769	1.083	110.9	108.0	-
$\mathrm{CCl_4}$	T_d	M06-2X	1.775	-	109.5	-	-
		MP2	1.759	-	109.5	-	-

Six of the eleven complexes were optimised at CCSD(T)/AVTZ. Optimisations at MP2/AVQZ had a tendency to underestimate bond lengths relative to CCSD(T).

There were only two instances where MP2 predicted a longer bond length than CCSD(T), both of which were C-H bond lengths where the hydrogen was involved in a hydrogen bond with the bromide. On average, MP2 predicted C-Cl bond lengths 0.013 Å shorter relative to CCSD(T). For the $Br^- \cdots CH_2Cl_2$ and $Br^- \cdots CHCl_3$ complexes, hydrogen bond lengths ($Br^- \cdots H$) and halogen bond lengths ($Br^- \cdots Cl$) calculated at MP2 are on average 0.068 Å and 0.079 Å shorter than at CCSD(T) respectively. For the halogen bonded $Br^- \cdots CH_3Cl$ complex, MP2 predicts a $Br^- \cdots Cl$ bond length 0.131 Å shorter than at CCSD(T), while the ion dipole complex has a $Br^- \cdots H$ bond length only 0.029 Å shorter than at CCSD(T).

At M06-2X/6-31+G(d,p), C-Cl and C-H bond lengths are relatively unchanged when compared to CCSD(T). M06-2X predicted $Br^- \cdots H$ bond lengths that are 0.044 Å and 0.022 Å shorter than CCSD(T) for the $Br^- \cdots CH_3Cl$ and $Br^- \cdots CHCl_3$ complexes respectively, whereas for the $Br^- \cdots CH_2Cl_2$ complex the $Br^- \cdots H$ bond length is found to be 0.048 Å longer than CCSD(T). Similar to MP2, M06-2X predicts the halogen bond in the $Br^- \cdots CH_3Cl$ complex to be 0.124 Å shorter than at CCSD(T). The $Br^- \cdots Cl$ bond lengths at M06-2X for the $Br^- \cdots CH_2Cl_2$ and $Br^- \cdots CHCl_3$ complexes are on average 0.031 Å shorter relative to CCSD(T). Further comments could be made on the performance of both MP2/AVQZ and M06-2X/6-31+G(d,p) once the remaining five complexes are optimised at CCSD(T)/AVTZ.

3.2.6 Dissociation and Vertical Detachment Energies

When calculating vertical detachment energies, a shift constant is applied to the split VDEs to give a better estimate of the $^2P_{3/2}$ and $^2P_{1/2}$ peaks that will be observed in experiment, as mentioned previously in the materials and methods chapter. The data presented in Table 3.8 is a summary of the shift constants each level of theory and basis set used in this project, calculated as the difference between the literature $^2P_{3/2}$ value and the theoretical split $^2P_{3/2}$ value.

Table 3.8: Calculation of energy shift constants for bromide and iodide, in eV.

	Method/Basis Set	VDE	Split VDE $^2P_{3/2}$	Split VDE $^2P_{1/2}$	Literature $^2P_{3/2}$	Shift
Br^-	M06-2X/6-31+G(d,p)	3.509	3.357	3.814	3.364	+0.007
	M06-2X/6-311++G(3df,3pd)	3.452	3.300	3.757		+0.064
	MP2/AVQZ	3.537	3.385	3.842		−0.021
	MP2/AV5Z	3.579	3.427	3.884		−0.063
	MP2/CBS	3.624	3.472	3.929		−0.108
	CCSD(T)/AVDZ	3.272	3.120	3.577		+0.244
	CCSD(T)/AVTZ	3.351	3.199	3.656		+0.165
	CCSD(T)/AVQZ	3.457	3.305	3.762		+0.059
	CCSD(T)/CBS	3.529	3.377	3.834		−0.013
I^-	MP2/AVQZ	3.372	3.058	4.000	3.059	+0.001
	MP2/AV5Z	3.418	3.104	4.046		−0.045
	MP2/CBS	3.469	3.155	4.097		−0.096
	CCSD(T)/AVDZ	3.107	2.793	3.735		+0.266
	CCSD(T)/AVTZ	3.180	2.866	3.808		+0.193
	CCSD(T)/AVQZ	3.300	2.986	3.928		+0.073
	CCSD(T)/CBS	3.379	3.065	4.007		−0.006

The M06-2X functional was used with two different basis sets, the first being the 6-31+G(d,p) basis set for optimisation and frequency calculations which has a corresponding shift value of +0.007 eV, while the other being the 6-311++G(3df,3pd) basis set which has a shift value of +0.064 eV. Both basis sets with the M06-2X functional underestimated the bromide $^2P_{3/2}$ state, with the 6-311++G(3df,3pd) basis set underestimating it by a larger magnitude. While not reported in Table 3.8, the M06-2X functional was also tested with the AVDZ, AVTZ and AVQZ basis sets, and resulted in shift values of +0.108, +0.157 and +0.174 eV respectively. This is an indicator that the M06-2X functional with increasing basis set size is divergent with respect to experimental bromide, i.e. calculated $^2P_{3/2}$ peak energies are increasingly underestimated with larger basis sets.

For MP2 calculations involving bromide, the shift values were calculated as −0.021 eV for the AVQZ basis set, −0.063 eV for the AV5Z basis set, and −0.108 eV when extrapolated to the CBS limit. Similarly, MP2 calculations involving iodide were found to have shift values of +0.001, −0.045 and −0.096 eV at AVQZ, AV5Z and CBS respectively. With the exception of iodide at AVQZ, MP2 calculations using a large basis set had a tendency to overestimate the $^2P_{3/2}$ peak position, unlike the M06-2X functional which had a tendency to underestimate the $^2P_{3/2}$ peak position. However, similar to the M06-2X functional, the MP2 shift values were shown to diverge relative to experimental halide peaks.

The shift values calculated for CCSD(T) calculations involving bromide were +0.244 eV for the AVDZ basis set, +0.165 eV for the AVTZ basis set, and +0.059 eV for the AVQZ basis set. For calculations involving iodide, the AVDZ, AVTZ and AVQZ shift values were found to be +0.266 eV, +0.193 eV and +0.073 eV respectively. When extrapolated to the CBS limit, the shift value decreases to −0.013 eV for calculations involving bromide, and −0.006 eV for calculations involving iodide. The small shift values indicate that CCSD(T)/CBS calculations are convergent relative to experimental halide peaks, which demonstrates the accuracy of CCSD(T) level of theory.

Table 3.9 presents a summary of dissociation energies and vertical detachment energies calculated for all halide chloromethane complexes in this project. The reported VDE values have all been corrected with respect to their shift constants found in Table 3.8, so any deviations between levels of theory are small.

At CCSD(T), the $^2P_{3/2}$ and $^2P_{1/2}$ electronic states of the hydrogen bonded $Br^- \cdots CH_3Cl$ complex were calculated to be 3.797 eV and 4.254 eV respectively, whereas the VDE

Table 3.9: Predicted dissociation energies and vertical detachment energies of halide chloromethane anion complexes.

		Method/Basis Set	D_0	VDE (eV)	
			(kJ mol^{-1})	$^2P_{3/2}$	$^2P_{1/2}$
$Br^- \cdots CH_3Cl$	ID	M06-2X/6-311++G(3df,3pd)	42.0	3.808	4.265
		MP2/CBS	41.2	3.787	4.244
		CCSD(T)/CBS^a	43.0	3.783	4.240
		CCSD(T)/CBS^b	44.6	3.797	4.254
$Br^- \cdots CH_3Cl$	XB	M06-2X/6-311++G(3df,3pd)	-5.0	3.293	3.750
		MP2/CBS	-3.1	3.293	3.750
		CCSD(T)/CBS^a	-3.6	3.288	3.745
		CCSD(T)/CBS^b	-3.3	3.283	3.740
$Br^- \cdots CH_2Cl_2$	HB	M06-2X/6-311++G(3df,3pd)	50.6	3.961	4.418
		MP2/CBS	57.3	3.989	4.446
		CCSD(T)/CBS^a	56.6	3.979	4.436
		CCSD(T)/CBS^b	56.6	3.960	4.417
$Br^- \cdots CH_2Cl_2$	XB	M06-2X/6-311++G(3df,3pd)	14.1	3.521	3.978
		MP2/CBS	16.1	3.505	3.962
		CCSD(T)/CBS^a	15.4	3.520	3.977
		CCSD(T)/CBS^b	15.7	3.502	3.959
$Br^- \cdots CHCl_3$	HB	M06-2X/6-311++G(3df,3pd)	64.5	4.130	4.587
		MP2/CBS	74.1	4.162	4.619
		CCSD(T)/CBS^a	72.1	4.148	4.605
		CCSD(T)/CBS^b	71.8	4.110	4.567
$Br^- \cdots CHCl_3$	XB	M06-2X/6-311++G(3df,3pd)	28.3	3.657	4.114
		MP2/CBS	32.0	3.715	4.172
		CCSD(T)/CBS^a	30.2	3.700	4.157
		CCSD(T)/CBS^b	30.7	3.684	4.141
$Br^- \cdots CHCl_3$	IID	M06-2X/6-311++G(3df,3pd)	6.8	3.378	3.835
		MP2/CBS	8.0	3.377	3.834
		CCSD(T)/CBS^a	6.2	3.370	3.827
$Br^- \cdots CCl_4$	XB	M06-2X/6-311++G(3df,3pd)	38.6	3.861	4.318
		MP2/CBS	45.7	3.896	4.353
		CCSD(T)/CBS^a	42.6	3.875	4.332
$Br^- \cdots CCl_4$	IID	M06-2X/6-311++G(3df,3pd)	19.4	3.526	3.983
		MP2/CBS	22.6	3.529	3.986
		CCSD(T)/CBS^a	19.6	3.518	3.975
$I^- \cdots CCl_4$	XB	MP2/CBS	41.1	3.452	4.394
		CCSD(T)/CBS^a	35.8	3.422	4.364
$I^- \cdots CCl_4$	IID	MP2/CBS	22.6	3.138	4.080
		CCSD(T)/CBS^a	17.3	3.123	4.065

[a] Calculated from MP2/AVQZ geometries

[b] Calculated from CCSD(T)/AVTZ geometries

values of the halogen bonded complex were calculated as 3.283 eV and 3.740 eV. The dissociation energies of the hydrogen bonded complex range between 41.2 kJ mol^{-1}

at MP2/CBS, and 44.6 kJ mol^{-1} at CCSD(T)/CBS. In contrast, the halogen bonded $Br^- \cdots CH_3Cl$ complex is the only system studied in this project to have a negative dissociation energy relative to its constituents (-3.3 kJ mol^{-1} at CCSD(T)/CBS), potentially indicating that this structure is a high lying local minimum on the potential energy surface. Future work on this system will involve finding a transition structure between the two complexes, which may involve the rotation of the CH_3Cl. While no photoelectron spectra have been recorded for $Br^- \cdots CH_3Cl$, the most likely structure to be observed experimentally is the hydrogen bonded complex, as the halogen bonded complex is very weak in comparison due to hydrogen atoms being poor at withdrawing electron density. This is evident through calculation of a Boltzmann distribution, where at 298 K the relative proportion of the halogen bonded complex would be negligible ($\approx 1\times10^{-8}$).

The hydrogen bonded $Br^- \cdots CH_2Cl_2$ complex is calculated to have peaks at 3.960 eV ($^2P_{3/2}$) and 4.417 eV ($^2P_{1/2}$), compared to the halogen bonded complex which is calculated to have peaks at 3.502 eV and 3.959 eV. While the $^2P_{3/2}$ peak of the hydrogen bonded complex overlaps with the halogen bonded $^2P_{1/2}$ peak, a lack of a peak at 3.502 eV or 4.417 eV in a photoelectron spectrum would distinguish the two complexes apart. From the spectrum in Figure 3.4, peaks are found at 3.98 eV and 4.44 eV, which indicates that the hydrogen bonded complex is the observed structure experimentally. Further evidence can be found by comparing the dissociation energies, which at CCSD(T) was calculated to be 56.6 kJ mol^{-1} and 15.7 kJ mol^{-1} for the hydrogen and halogen bonded complexes respectively. In the halogen bonded complex, the non-interacting chlorine atom withdraws electron density away from the chlorine atom that is interacting with the bromide, allowing the halogen bond to stabilise, albeit weakly compared with the hydrogen bond.

At CCSD(T), the hydrogen bonded $Br^- \cdots CHCl_3$ complex has VDE peaks at 4.110 eV and 4.567 eV, which agree with the $^2P_{3/2}$ and $^2P_{1/2}$ peaks found at 4.09 eV and 4.51 eV in the bromide trichloromethane photoelectron spectrum in Figure 3.5. While the $^2P_{1/2}$ VDE of the halogen bonded complex overlaps with the $^2P_{3/2}$ peak in the spectrum, the $^2P_{3/2}$ peak at 3.700 eV, as well as the peaks at 3.370 eV and 3.827 eV corresponding with the ion induced dipole complex, all have no presence in the spectrum. This eliminates the possibility that the $Br^- \cdots CHCl_3$ complex observed in the photoelectron spectrum interacts via halogen bonding or an ion induced dipole. The large dissociation energy calculated from CCSD(T)/AVTZ geometries (72.1 kJ mol^{-1}) associated with the hydrogen bonded complex is a result of the three chlorine atoms polarising the molecule, such that the positive dipole at the hydrogen stabilises the interaction with the bromide. Similarly, a dissociation energy of 30.7 kJ mol^{-1} for the halogen bonded complex arises due to the non-interacting chlorine atoms pulling electron density away from the interacting chlorine, hence stabilising the halogen bond. However, despite the halogen bond being relatively stable, the hydrogen bond interaction is favoured, hence why it is the structure observed in the photoelectron spectrum.

At CCSD(T), the $^2P_{3/2}$ and $^2P_{1/2}$ peaks of the halogen bonded $Br^- \cdots CCl_4$ complex are at 3.875 eV and 4.332 eV respectively, whereas the peaks associated with the ion induced dipole complex are at 3.518 eV and 3.975 eV. The two peaks calculated for the halogen bonded complex agree with the two peaks (3.85 eV, 4.29 eV) found in the photoelectron spectrum of $Br^- \cdots CCl_4$ in Figure 3.6, indicating that the halogen bonded complex is the observed structure. A dissociation energy of 42.6 kJ mol^{-1} is calculated for the halogen bond interaction, stabilised by the three non-interacting chlorine atoms pulling electron density away from the interacting chlorine atom, resulting in the strongest halogen bond of the bromide chloromethane complexes. The ion induced dipole complex occurs when the bromide induces a slight positive dipole on the neutral CCl_4 molecule. Electron density on the three interacting chlorine atoms is pulled towards the non-interacting chlorine, resulting in a complex with a dissociation energy of 19.6 kJ mol^{-1}. However, the halogen bond interaction is favoured of the two complexes, thus being the observed structure in experiment.

The calculated VDE peaks of the halogen bonded $I^- \cdots CCl_4$ complex are at 3.422 eV and 4.364 eV, while the peaks associated with the ion induced dipole complex are calculated as 3.123 eV and 4.065 eV. Despite no photoelectron spectra to compare to, the halogen bonded complex is likely to be the observed structure, given that the halogen bonded complex was the observed structure for $Br^- \cdots CCl_4$. From calculation of a Boltzmann distribution, the relative proportion of the ion induced dipole complex at 298 K would be negligible ($\approx 6 \times 10^{-4}$), and temperatures of 20-30 K are achieved when conducting experiments, hence the relative proportion would be even lower, further supporting the halogen bonded structure being observed in experiment. Dissociation energies of 35.8 kJ mol^{-1} and 17.3 kJ mol^{-1} are calculated at CCSD(T) for the halogen bonded and ion induced dipole complexes respectively, which are both lower in energy than their bromide counterparts. Iodide is less electronegative than bromide, so electron density is more easily able to be withdrawn from iodide compared to bromide. This results in the stability of the interaction decreasing relative to bromide, as chlorine atoms pull more electron density away from the iodide, hence a lower dissociation energy is calculated.

At M06-2X/6-311++G(3df,3pd), a dissociation energy of 50.6 kJ mol^{-1} was calculated for the hydrogen bonded $Br^- \cdots CH_2Cl_2$ complex, which deviates from the

CCSD(T)/CBS value by 6.0 kJ mol^{-1}. Similarly, the M06-2X dissociation energy of the hydrogen bonded $Br^- \cdots CHCl_3$ complex differs to CCSD(T) by 7.3 kJ mol^{-1}, and both MP2/CBS dissociation energies of the $I^- \cdots CCl_4$ complex differ by 5.3 kJ mol^{-1} relative to CCSD(T). The commonality between these four deviations is that they are all greater than chemical accuracy, i.e. the dissociation energies calculated are inaccurate relative to CCSD(T). M06-2X consistently underestimated the dissociation energies of both hydrogen and halogen bonded systems, whereas MP2 typically overestimated dissociation energies, with the one exception being the $Br^- \cdots CH_3Cl$ complex interacting via an ion dipole which it underestimated. Generally, there was minimal difference ($\leq$0.5 kJ mol^{-1}) between the dissociation energies calculated at CCSD(T)/CBS when calculated from MP2/AVQZ or CCSD(T)/AVTZ geometries, with the exception being the hydrogen bonded $Br^- \cdots CH_3Cl$ complex which differed by 1.6 kJ mol^{-1}.

3.3 Hydrogen Bonding versus Halogen Bonding

The question proposed in the title of this project asks whether a hydrogen bond or a halogen bond would be favoured between a halide and the four chloromethane molecules. To answer this question, every possible halide chloromethane structure was tested, which comprised of every combination of interaction the halide could undergo with hydrogen and chlorine. This included optimising structures where the halide was appended to one atom (H or Cl), appended to two atoms (2H, 2Cl, or H and Cl), or appended to three atoms (3H, 3Cl, 2H and Cl, or H and 2Cl), depending on the chloromethane that the halide was interacting with. These geometry optimisations were performed at MP2/AVDZ, as stated in the materials and methods chapter.

Of the eleven resulting structures, only two feature the halide appending to one hydrogen atom in a typical hydrogen bond motif ($\mathrm{Br^- \cdots CH_2Cl_2}$ and $\mathrm{Br^- \cdots CHCl_3}$), whereas each halide chloromethane system has one structure that involves the halide appending to one chlorine atom in a halogen bond motif. While bromide is found to interact via an ion dipole with the three hydrogen atoms of monochloromethane, the interaction is not a typical hydrogen bond, and will therefore not be discussed here.

Of the two hydrogen bonded complexes, the general trend observed was that with increased chlorine substitution, hydrogen bond strength increased. This is because chlorine atoms increase the polarisation of the molecule, such that a positive dipole is present near the hydrogen atoms, and a negative dipole is present near the chlorine atoms. Increasing the number of chlorine atoms will increase the magnitude of the negative dipole, and hence will also increase the magnitude of the positive dipole. The stability of the interaction of a halide with the hydrogen will increase as the magnitude of the positive dipole increases, hence increasing the hydrogen bond strength. The predicted dissociation energies at CCSD(T) from MP2/AVQZ geometries provide evidence of this behaviour, with $\mathrm{Br^- \cdots CHCl_3}$ at 72.1 kJ mol^{-1} and $\mathrm{Br^- \cdots CH_2Cl_2}$ at 56.6 kJ mol^{-1}.

Increasing the chlorine substitution in the chloromethane molecule increases the strength of a halogen bond, as increasing the number of non-interacting chlorine atoms will also increase the electron density withdrawing capacity of the molecule, hence increasing the magnitude of the σ-hole, and thus allowing more stable halogen bond interactions. This is evident from the predicted dissociation energies at CCSD(T) from MP2/AVQZ geometries, with $Br^- \cdots CCl_4$ at 42.6 kJ mol^{-1}, $Br^- \cdots CHCl_3$ at 30.2 kJ mol^{-1}, $Br^- \cdots CH_2Cl_2$ at 15.4 kJ mol^{-1}, and $Br^- \cdots CH_3Cl$ at -3.6 kJ mol^{-1}. The negative dissociation energy of $Br^- \cdots CH_3Cl$ indicates that this particular halogen bond interaction is very unfavourable, as hydrogen atoms are poor at withdrawing electron density, as has been stated previously in this thesis.

As a negatively charged species will more favourably interact with a positive region, such as a hydrogen, hydrogen bonding interactions will be dominant over halogen bonding interactions, which require highly electronegative atoms, such as fluorine and chlorine, to withdraw electron density from another halogen to favourably interact. This is observed from the photoelectron spectra in this project, where $Br^- \cdots CH_2Cl_2$ and $Br^- \cdots CHCl_3$ were determined to be interacting via hydrogen bonding, whereas the $Br^- \cdots CCl_4$ complex, a system with no hydrogen atoms present, was determined to be interacting via halogen bonding. The experimental E_{stab} values of 0.62 eV and 0.73 eV for the $^2P_{3/2}$ peaks associated with $Br^- \cdots CH_2Cl_2$ and $Br^- \cdots CHCl_3$ respectively are larger than E_{stab} value of 0.49 eV associated with the $Br^- \cdots CCl_4$ $^2P_{3/2}$ peak, indicating that a hydrogen bond interaction provides more of a stabilising effect to bare bromide than a halogen bond interaction, further evidence that the hydrogen bond interaction is favoured.

Interestingly, from predicted dissociation energies at CBS from CCSD(T)/AVTZ geometries, the hydrogen bonded $Br^- \cdots CH_2Cl_2$ complex requires 40.9 kJ mol^{-1} more energy to dissociate than the halogen bonded $Br^- \cdots CH_2Cl_2$ complex, while the hydrogen bonded $Br^- \cdots CHCl_3$ complex requires 41.1 kJ mol^{-1} more energy to dissociate than the halogen bonded $Br^- \cdots CHCl_3$ complex, for an average of 41.0 kJ mol^{-1}. This gives an estimate as to how much stronger a hydrogen bond is compared to a halogen bond for these specific complexes.

3.4 Literature Comparison

Of the halide chloromethane complexes studied in this project, two experimental enthalpy of formation energies have been found in the literature. For the $Br^- \cdots CH_3Cl$ complex, a ΔH° value of -10.9±1.0 kcal mol^{-1} (-45.6±4.2 kJ mol^{-1}) is reported by the Li group(52), whereas for the $Br^- \cdots CHCl_3$ complex, a ΔH° value of -15.8 kcal mol^{-1} (-66.1 kJ mol^{-1}) is found by Giles and Grimsrud(23). While dissociation energies found in this project cannot be directly compared to these experimentally determined ΔH° values, future work can be undertaken to calculate theoretical thermodynamic properties of halide chloromethane complexes.

The Wild group studied the two $Cl^- \cdots CCl_4$ complexes(47), one interacting via a halogen bond and one via an ion induced dipole. At MP2/AVQZ, the halogen bond length was found to be 2.780 Å, shorter than the $Br^- \cdots CCl_4$ and $I^- \cdots CCl_4$ halogen bond lengths of 2.928 Å and 3.171 Å that were found in this project respectively. The halide to chlorine bond length was also shown to increase for the ion induced dipole complexes, with lengths of 3.563 Å, 3.694 Å, and 3.966 Å for chloride, bromide, and iodide respectively. The predicted dissociation energies at CCSD(T)/CBS follow a trend for the halogen bonded complexes, with chloride interacting the strongest (46.7 kJ mol^{-1}), followed by bromide (42.6 kJ mol^{-1}), and lastly iodide interacting the weakest (35.8 kJ mol^{-1}) with the tetrachloromethane molecule. Also following the trend, the dissociation energies of the ion induced dipole complexes are 20.2 kJ mol^{-1} for chloride, 19.6 kJ mol^{-1} for bromide and 17.3 kJ mol^{-1} for iodide. However, it must be noted that the calculations involving chloride were extrapolated to the CBS limit using the W2w protocol, whereas calculations in this project were extrapolated using the W1w protocol, which could affect the results slightly.

At MP2/6-31+G(d) level of theory, Glukhovtsev et al. found a $Br^- \cdots C$ bond length of 3.457 Å for the hydrogen bonded $Br^- \cdots CH_3Cl$ complex(48). In comparison, at CCSD(T)/AVTZ the $Br^- \cdots C$ bond length found in this project is 3.272 Å, indicating that the distance at which bromide interacts with monochloromethane is shorter than previously calculated. At HF/3-21G* theory, Kobychev et al. found $I^- \cdots Cl$ bond lengths of 3.427 Å for the halogen bonded $I^- \cdots CCl_4$ complex, and 4.845 Å for the ion induced dipole $I^- \cdots CCl_4$ complex(49). The two bond lengths were found to be 0.256 Å and 0.879 Å longer than the corresponding bond lengths found at MP2/AVQZ in this project respectively.

Chapter 4

Conclusions and Future Work

The hydrogen bond, halogen bond and ion induced dipole interactions of halide chloromethane complexes have been studied through experimental and computational techniques. Photoelectron spectra of the $Br^- \cdots CH_2Cl_2$, $Br^- \cdots CHCl_3$ and $Br^- \cdots CCl_4$ complexes were recorded, and used to rationalise which interaction was most likely to occur in experiment.

To answer the question proposed in the title of this project, complexes interacting via hydrogen bonds were the favoured structure, unless no hydrogen atoms were present, such as in the case of tetrachloromethane, where the halogen bond interaction was favoured. This was evident from *ab initio* calculations, where a total of eleven anion complexes were optimised at MP2/AVQZ, six of which were further optimised at CCSD(T)/AVTZ level of theory. Calculations of theoretical vertical detachment energies and dissociation energies were extrapolated to the CBS limit to give a highly accurate prediction of the intermolecular interactions that arise in halide chloromethane complexes.

Calculations using the M06-2X functional and 6-311++G(3df,3pd) basis set, as well as calculations extrapolated to MP2/CBS from MP2/AVXZ basis sets were compared to CCSD(T)/CBS to determine how well each level of theory performed. MP2 had a tendency to overestimate dissociation and vertical detachment energies, and underestimate bond lengths, whereas M06-2X had a tendency to underestimate energies, and underestimate the bond lengths involved in the weak intermolecular interactions. While the M06-2X functional performs decently in terms of describing the halogen bonding interaction as claimed by Zhang et al.(72), CCSD(T) level of theory predicts more accurate results, which was shown from the two instances where M06-2X underpredicted dissociation energies that deviated by more than chemical accuracy relative to CCSD(T), as well as the divergence of shift constants at larger basis sets. Additional calculations using the M06-2X functional could be done in the future with Dunning's basis sets to further test Zhang's claim.

Future work on these halide chloromethane complexes would involve optimising the remainder of the anion complexes at CCSD(T)/AVTZ, and performing geometry optimisations on the neutral complexes so that theoretical E_{stab} values can be determined and compared to experiment. Another avenue of work is the optimisation of transition structures to determine theoretical barrier heights, such as the rotation of the monochloromethane in the $Br^- \cdots CH_3Cl$ system. Photoelectron spectra for $Br^- \cdots CH_3Cl$ and $I^- \cdots CCl_4$ will be recorded in the future, and slow electron velocity imaging (SEVI) experiments are another potential avenue, which would increase the resolution of the resulting photoelectron spectra.

References

1. Valach R. The origin of the gaseous form of natural atmospheric chlorine. Tellus. 1967;19(3):509-16. Available from: doi:10.1111/j.2153-3490.1967.tb01505.x

2. Moldanová J, Ljungström E. Sea-salt aerosol chemistry in coastal area: A model study. J Geophys Res. 2001;106(D1):1271-96. Available from: doi:10.1029/2000JD900462

3. Rowland, FS. Chlorofluorocarbons and the Depletion of Stratospheric Ozone. Am Sci. 1987;77(1):36-45. Available from: www.jstor.org/stable/27855550

4. Wayne, RP. Chemistry of Atmospheres. 3rd ed. New York: Oxford University Press; 2000. 165 p.

5. Hossaini R, Chipperfield MP, Monge-Sanz BM, Richards NAD, Atlas E, Blake DR. Bromoform and dibromomethane in the tropics: a 3-D model study of chemistry and transport. Atmos Chem Phys. 2010;10:719-35. Available from: doi:10.5194/acp-10-719-2010

6. Saiz-Lopez A, Plane JMC, Baker AR, Carpenter LJ, von Glasow R, Gómez Martín JC, et al. Atmospheric Chemistry of Iodine. Chem Rev. 2012;112:1773-804. Available from: doi:10.1021/cr200029u

7. Tsai W-T. Fate of Chloromethanes in the Atmospheric Environment: Implications for Human Health, Ozone Formation and Depletion, and Global Warming Impacts. Toxics. 2017;5(4):23-35. Available from: doi:10.3390/toxics5040023

8. Karton A, Kettner M, Wild DA. Sneaking up on the Criegee intermediate from below: Predicted photoelectron spectrum of the CH_2OO^- anion and W3-F12 electron affinity of CH_2OO. Chem Phys Lett. 2013;585:15-20. Available from: doi:10.1016/j.cplett.2013.08.075

9. Dong F, Heinbuch S, Rocca JJ, Bernstein ER. Dynamics and fragmentation of van der Waals clusters: $(H_2O)_n$, $(CH_3OH)_n$, and $(NH_2)_n$ upon ionization by a 26.5 eV soft x-ray laser. J Chem Phys. 2006;124(22):224319. Available from: doi:10.1063/1.2202314

10. London F. The general theory of molecular forces. Trans Faraday Soc. 1937;33:8b-26. Available from: doi:10.1039/TF937330008B

11. Wolters LP, Bickelhaupt FM. Halogen Bonding versus Hydrogen Bonding: A Molecular Orbital Perspective. ChemistryOpen. 2012;1(2):96-105. Available from: doi:10.1002/open.201100015

12. Mulliken RS. Molecular Compounds and their Spectra. III. The Interaction of Electron Donors and Acceptors. J Phys Chem. 1952;56(7):801–22. Available from: doi:10.1021/j150499a001

13. Pauli W. Über den Zusammenhang des Abschlusses der Elektronengruppen im Atom mit der Komplexstruktur der Spektren. Z Physik. 1925;31:765-83. Available from: doi:10.1007/BF02980631

14. Mao Y, Horn PR, Head-Gordon M. Energy decomposition analysis in an adiabatic picture. Phys Chem Chem Phys. 2017;19:5944-58. Available from: doi:10.1039/c6cp08039a

15. Riley KE, Hobza P. The relative roles of electrostatics and dispersion in the stabilization of halogen bonds. Phys Chem Chem Phys. 2013;15(41):17742-51. Available from: doi:10.1039/c3cp52768a

16. Politzer P, Murray JS, Clark T, Resnati G. The σ-hole revisited. Phys Chem Chem Phys. 2017;19:32166-78. Available from: doi:10.1039/c7cp06793c

17. Ramasubbu N, Parthasarathy R, Murray-Rust P. Angular preferences of intermolecular forces around halogen centers: preferred directions of approach of electrophiles and nucleophiles around carbon-halogen bond. J Am Chem Soc. 1986;108(15):4308-14. Available from: doi:10.1021/ja00275a012

18. Politzer P, Murray JS. Halogen Bonding: An Interim Discussion. ChemPhysChem. 2013;14:278-94. Available from: doi:10.1002/cphc.201200799

19. Clark T, Hennemann M, Murray JS, Politzer P. Halogen bonding: the σ-hole. J Mol Model. 2007;13:291-6. Available from: doi:10.1007/s00894-006-0130-2

20. Wolf ME, Zhang B, Turney JM, Schaefer III HF. A comparison between hydrogen and halogen bonding: the hypohalous acid–water dimers, HOX...H_2O (X = F, Cl, Br). Phys Chem Chem Phys. 2019;21:6160-70. Available from: doi:10.1039/c9cp00422j

21. Quiñonero D, Frontera A. Hydrogen Bond versus Halogen Bond in HXO_n (X

= F, Cl, Br, and I) Complexes with Lewis Bases. Inorganics. 2019;7(1):9. Available from: doi:10.3390/inorganics7010009

22. Keesee RG, Castleman Jr AW. Thermochemical Data on Gas-Phase Ion-Molecule Association and Clustering Reactions. J Phys Chem Ref Data. 2009;15(3):1011-986. Available from: doi:10.1063/1.555757

23. Giles K, Grimsrud EP. Measurements of equilibria and reactivity of cluster ions at atmospheric pressure: reactions of $Cl^-(CHCl_3)_{0-2}$ with methyl bromide and methyl iodide. J Phys Chem. 1993;97(7):1318-23. Available from: doi:10.1021/j100109a012

24. Lapere KML, McKinley AJ, Wild DA. Anion Photoelectron Spectroscopy and High Level Ab Initio Calculations of the Halide–Nitric Oxide Dimer Complexes. Aust J Chem. 2018;71(4):265-71. Available from: doi:10.1071/CH17581

25. Kammrath A, Verlet JRR, Griffin GB, Neumark DM. Photoelectron spectroscopy of large $(\text{water})_n^-$ (n = 50–200) clusters at 4.7 eV. J Chem Phys. 2006;125(7):076101. Available from: doi:10.1063/1.2217745

26. DeLuca MJ, Niu B, Johnson MA. Photoelectron spectroscopy of $(CO_2)_n^-$ clusters with $2 \leq n \leq 13$: Cluster size dependence of the core molecular ion. J Chem Phys. 1988;88(9):5857-63. Available from: doi:10.1063/1.454548

27. Brehm B, Gusinow MA, Hall JL. Electron Affinity of Helium Via Laser Photodetachment of its Negative Ion. Phys Rev Lett. 1967;19(13):737-41. Available from: doi:10.1103/PhysRevLett.19.737

28. Condon EU. Nuclear Motions Associated with Electron Transitions in

Diatomic Molecules. Phys Rev. 1928;32:858-72. Available from: doi:10.1103/PhysRev.32.858

29. Lapere KML. Anion Photoelectron Spectroscopy of Halide Complexes and Clusters [Dissertation]. [Perth (AU)]: University of Western Australia; 2015.

30. Born M, Oppenheimer R. Zur Quantentheorie der Molekeln. Ann Phys. 1927;389(20):457-84. Available from: doi:10.1002/andp.19273892002

31. Nesbet RK. Approximate Methods in the Quantum Theory of Many-Fermion Systems. Revs Modern Phys. 1961;33(1):28-36. Available from: doi:10.1103/RevModPhys.33.28

32. Slater JC. A Simplification of the Hartree-Fock Method. Phys Rev. 1951;81(3):385-90. Available from: doi:10.1103/PhysRev.81.385

33. Møller C, Plesset MS, Note on an Approximation Treatment for Many-Electron Systems. Phys Rev. 1934;46:618-22. Available from: doi:10.1103/PhysRev.46.618

34. Jung Y, Lochan RC, Dutoi AD, Head-Gordon M. Scaled opposite-spin second order Møller–Plesset correlation energy: An economical electronic structure method. J Chem Phys. 2004;121(20):9793-802. Available from: doi:10.1063/1.1809602

35. Grimme S. Improved second-order Møller–Plesset perturbation theory by separate scaling of parallel- and antiparallel-spin pair correlation energies. J Chem Phys. 2003;118(20):9095-102. Available from: doi:10.1063/1.1569242

36. Wilson AK, van Mourik T, Dunning Jr TH. Gaussian basis sets for use in correlated molecular calculations. VI. Sextuple zeta correlation consistent

basis sets for boron through neon. J Mol Struc-Theochem. 1996;388:339-49. Available from: doi:10.1016/S0166-1280(96)80048-0

37. Bartlett RJ, Musial M. Coupled-cluster theory in quantum chemistry. Revs Modern Phys. 2007;79:291-352. Available from: doi:10.1103/RevModPhys.79.291

38. Bak KL, Jørgensen P, Olsen J, Helgaker T, Klopper W. Accuracy of atomization energies and reaction enthalpies in standard and extrapolated electronic wave function/basis set calculations. J Chem Phys. 2000;112(21):9229-42. Available from: doi:10.1063/1.481544

39. Binkley JS, Pople JA, Hehre WJ. Self-consistent molecular orbital methods. 21. Small split-valence basis sets for first-row elements. J Am Chem Soc. 1980;102(3):939-47. Available from: doi:10.1021/ja00523a008

40. Guseinov II, Analytical evaluation of three- and four-center electron-repulsion integrals for Slater-type orbitals. J Chem Phys. 1978;69(11):4990-4. Available from: doi:10.1063/1.436488

41. Hehre WJ, Stewart RF, Pople JA. Self-Consistent Molecular-Orbital Methods. I. Use of Gaussian Expansions of Slater-Type Atomic Orbitals. J Chem Phys. 1969;51(6):2657-64. Available from: doi:10.1063/1.1672392

42. Papajak E, Leverentz HR, Zheng J, Truhlar DG. Efficient Diffuse Basis Sets: cc-pVxZ+ and maug-cc-pVxZ. J Chem Theory Comput. 2009;5:1197-202. Available from: doi:10.1021/ct800575z

43. Spitznagel GW, Clark T, von Ragué Schleyer P, Hehre WJ. An evaluation of the performance of diffuse function-augmented basis sets for second row

elements, Na-Cl. J Comput Chem. 1987;8:1109-16. Available from: doi:10.1002/jcc.540080807

44. Butler PR, Ellis AM. Application of the Truhlar basis set extrapolation procedure to ab initio calculations on van der Waals complexes. Mol Phys. 2001;99(6):525-9. Available from: doi:10.1080/00268970010018855

45. Hariharan PC, Pople JA. The influence of polarization functions on molecular orbital hydrogenation energies. Theoret Chim Acta. 1973;28:213-22. Available from: doi:10.1007/BF00533485

46. Schwerdtfeger P. The Pseudopotential Approximation in Electronic Structure Theory. ChemPhysChem. 2011;12:3143-55. Available from: doi:10.1002/cphc.201100387

47. Corkish TR, Haakansson CT, McKinley AJ, Wild DA. The Structure of CCl_5^- in the Gas Phase. J Phys Chem Lett. 2019;10:5338-42. Available from: doi:10.1021/acs.jpclett.9b02242

48. Glukhovtsev MN, Pross A, Radom L. Gas-Phase Non-Identity S_N2 Reactions of Halide Anions with Methyl Halides: A High-Level Computational Study. J Am Chem Soc. 1996;118:6273-84. Available from: doi:10.1021/ja953665n

49. Kobychev VB, Vitkovskaya NM, Abramov AV, Timokhin BV. Quantum-Chemical Study of Halophilic Interactions: III. Ab initio Study of the Attack of Tetrachloromethane by Halide Ions. Russ J Gen Chem. 1999;69(5):788-93.

50. Hiraoka K, Mizuno T, Iino T, Eguchi D. Characteristic Changes of Bond Energies for Gas-Phase Cluster Ions of Halide Ions with Methane and

Chloromethanes. J Phys Chem A. 2001;105:4887-93. Available from: doi:10.1021/jp010143n

51. Caldwell GW, Masucci JA, Ikonomou MG. Negative ion chemical ionization mass spectrometry—binding of molecules to bromide and iodide anions. Org Mass Spectrom. 1989;24(1):8-24. Available from: doi:10.1002/oms.1210240103

52. Li C, Ross P, Szulejko JE, McMahon TB. High-Pressure Mass Spectrometric Investigations of the Potential Energy Surfaces of Gas-Phase S_N2 Reactions. J Am Chem Soc. 1996;118:9360-7. Available from: doi:10.1021/ja960565o

53. Wiley WC, McLaren IH. Time-of-Flight Mass Spectrometer with Improved Resolution. Rev Sci Instrum. 1955;26(12):1150-7. Available from: doi:10.1063/1.1715212

54. LaMacchia RJ. Towards Anion Photoelectron Spectroscopy of Complexes and Clusters [Honours Thesis]. [Perth (AU)]: University of Western Australia; 2008.

55. Kettner M. Aspects of gas-phase anion spectroscopy [Dissertation]. [Perth (AU)]: University of Western Australia; 2015.

56. Cheshnovsky O, Yang SH, Pettiette CL, Craycraft MJ, Smalley RE. Magnetic time-of-flight photoelectron spectrometer for mass-selected negative cluster ions. Rev Sci Instrum. 1987;58(11):2131-7. Available from: doi:10.1063/1.1139475

57. Blondel C, Cacciani P, Delsart C, Trainham R. High-resolution determination of the electron affinity of fluorine and bromine using crossed

ion and laser beams. Phys Rev A. 1989;40(7):3698-702. Available from: doi:10.1103/PhysRevA.40.3698

58. Peláez RJ, Blondel C, Delsart C, Drag C. Pulsed photodetachment microscopy and the electron affinity of iodine. J Phys B. 2009;42(12):125001. Available from: doi:10.1088/0953-4075/42/12/125001

59. Sansonetti JE, Martin WC, Young SL. Handbook of Basic Atomic Spectroscopic Data (version 1.1.3). 2013. Available from: doi:10.18434/T4FW23

60. Gaussian 09, Revision D.01, M. J. Frisch, G. W. Trucks, H. B. Schlegel, G. E. Scuseria, M. A. Robb, J. R. Cheeseman, G. Scalmani, V. Barone, B. Mennucci, G. A. Petersson, H. Nakatsuji, M. Caricato, X. Li, H. P. Hratchian, A. F. Izmaylov, J. Bloino, G. Zheng, J. L. Sonnenberg, M. Hada, M. Ehara, K. Toyota, R. Fukuda, J. Hasegawa, M. Ishida, T. Nakajima, Y. Honda, O. Kitao, H. Nakai, T. Vreven, J. A. Montgomery, Jr., J. E. Peralta, F. Ogliaro, M. Bearpark, J. J. Heyd, E. Brothers, K. N. Kudin, V. N. Staroverov, T. Keith, R. Kobayashi, J. Normand, K. Raghavachari, A. Rendell, J. C. Burant, S. S. Iyengar, J. Tomasi, M. Cossi, N. Rega, J. M. Millam, M. Klene, J. E. Knox, J. B. Cross, V. Bakken, C. Adamo, J. Jaramillo, R. Gomperts, R. E. Stratmann, O. Yazyev, A. J. Austin, R. Cammi, C. Pomelli, J. W. Ochterski, R. L. Martin, K. Morokuma, V. G. Zakrzewski, G. A. Voth, P. Salvador, J. J. Dannenberg, S. Dapprich, A. D. Daniels, O. Farkas, J. B. Foresman, J. V. Ortiz, J. Cioslowski, and D. J. Fox, Gaussian, Inc., Wallingford CT, 2013.

61. CFOUR, a quantum chemical program package written by J.F. Stanton, J.

Gauss, L. Cheng, M.E. Harding, D.A. Matthews, P.G. Szalay with contributions from A.A. Auer, R.J. Bartlett, U. Benedikt, C. Berger, D.E. Bernholdt, Y.J. Bomble, O. Christiansen, F. Engel, R. Faber, M. Heckert, O. Heun, C. Huber, T.-C. Jagau, D. Jonsson, J. Jusélius, K. Klein, W.J. Lauderdale, F. Lipparini, T. Metzroth, L.A. Mück, D.P. O'Neill, D.R. Price, E. Prochnow, C. Puzzarini, K. Ruud, F. Schiffmann, W. Schwalbach, C. Simmons, S. Stopkowicz, A. Tajti, J. Vázquez, F. Wang, J.D. Watts and the integral packages MOLECULE (J. Almlöf and P.R. Taylor), PROPS (P.R. Taylor), ABACUS (T. Helgaker, H.J. Aa. Jensen, P. Jørgensen, and J. Olsen), and ECP routines by A. V. Mitin and C. van Wüllen. For the current version, see http://www.cfour.de.

62. Dunning TH. Gaussian basis sets for use in correlated molecular calculations. I. The atoms boron through neon and hydrogen. J Chem Phys. 1989;90(2):1007-23. Available from: doi:10.1063/1.456153

63. Kendall RA, Dunning TH. Electron affinities of the first-row atoms revisited. Systematic basis sets and wave functions. J Chem Phys. 1992;96(9):6796-806. Available from: doi:10.1063/1.462569

64. Woon DE, Dunning TH. Gaussian basis sets for use in correlated molecular calculations. III. The atoms aluminum through argon. J Chem Phys. 1993;98(2):1358-71. Available from: doi:10.1063/1.464303

65. Peterson KA, Woon DE, Dunning TH. Benchmark calculations with correlated molecular wave functions. IV. The classical barrier height of the $H+H_2 \rightarrow H_2+H$ reaction. J Chem Phys. 1994;100(10):7410-5. Available from: doi:10.1063/1.466884

66. Pritchard BP, Altarawy D, Didier B, Gibson TD, Windus TL. A New Basis Set Exchange: An Open, Up-to-date Resource for the Molecular Sciences Community. J Chem Inf Model. 2019;59(11):4814-20. Available from: doi:10.1021/acs.jcim.9b00725

67. Zhao Y, Truhlar DG. The M06 suite of density functionals for main group thermochemistry, thermochemical kinetics, noncovalent interactions, excited states, and transition elements: two new functionals and systematic testing of four M06-class functionals and 12 other functionals. Theor Chem Account. 2008;120:215-41. Available from: doi:10.1007/s00214-007-0310-x

68. Hehre WJ, Ditchfield R, Pople JA. Self-Consistent Molecular Orbital Methods. XII. Further Extensions of Gaussian-Type Basis Sets for Use in Molecular Orbital Studies of Organic Molecules. J Chem Phys. 1972;56(5):2257-61. Available from: doi:10.1063/1.1677527

69. Rassolov VA, Ratner MA, Pople JA, Redfern PC, Curtiss LA. 6-31G* basis set for third-row atoms. J Comput Chem. 2001;22(9):976-84. Available from: doi:10.1002/jcc.1058

70. McLean AD, Chandler GS. Contracted Gaussian basis sets for molecular calculations. I. Second row atoms, Z=11–18. J Chem Phys. 1980;72(10):5639-48. Available from: doi:10.1063/1.438980

71. Curtiss LA, McGrath MP, Blaudeau J-P, Davis NE, Binning RC, Radom L. Extension of Gaussian-2 theory to molecules containing third-row atoms Ga–Kr. J Chem Phys. 1995;103:6104-13. Available from: doi:10.1063/1.470438

72. Zhang X, Liu G, Ciborowski S, Wang W, Gong C, Yao Y, Bowen K. Spectroscopic Measurement of a Halogen Bond Energy. Angew Chem Int Ed. 2019;58:11400-3. Available from: doi:10.1002/anie.201906279

73. Karton A, Martin JML. Comment on: "Estimating the Hartree–Fock limit from finite basis set calculations" [Jensen F (2005) Theor Chem Acc 113:267]. Theor Chem Acc. 2006;115:330-3. Available from: doi:10.1007/s00214-005-0028-6

74. Karton A, Martin JML. Explicitly correlated Wn theory: W1-F12 and W2-F12. J Chem Phys. 2012;136(12):124114. Available from: doi:10.1063/1.3697678

75. Helgaker T, Klopper W, Koch H, Noga J. Basis-set convergence of correlated calculations on water. J Chem Phys. 1997;106(23):9639-46. Available from: doi:10.1063/1.473863

76. Haakansson CT, Corkish TR, Watson PD, McKinley AJ, Wild DA. The bromide-bromomethyl radical dimer complex: Anion photoelectron spectroscopy and CCSD(T) calculations. Chem Phys Lett. 2020;761;138060. Available from: doi:10.1016/j.cplett.2020.138060

Appendix A

Data and Tables

Table A.1: Energies calculated for chloromethane molecules at M06-2X/6-311++G(3df,3pd) level from optimised M06-2X/6-31+G(d,p) geometries.

	zpe (kJ mol^{-1})	M06-2X E_h (Hartree)
CH_3Cl	100.27	-500.1002810
CH_2Cl_2	78.51	-959.6995486
$CHCl_3$	53.48	-1419.2950432
CCl_4	25.24	-1878.8842858

Table A.2: Energies calculated for chloromethane molecules at MP2 level from optimised MP2/AVQZ geometries.

	zpe	MP2 E_h (Hartree)		
	(kJ mol^{-1})	QZ	5Z	CBS
CH_3Cl	100.51	-499.5631988	-499.5753993	-499.5871984
CH_2Cl_2	78.33	-958.7001248	-958.7200676	-958.7395711
$CHCl_3$	53.16	-1417.835015	-1417.862742	-1417.8899816
CCl_4	25.68	-1876.964948	-1877.000546	-1877.0356205

Table A.3: Energies calculated for chloromethane molecules at CCSD(T) level from optimised MP2/AVQZ geometries.

	CCSD(T) E_h (Hartree)			
	DZ	TZ	QZ	CBS
CH_3Cl	-499.4713289	-499.5778170	-499.6080480	-499.6255794
CH_2Cl_2	-958.5478960	-958.7147167	-958.7643267	-958.7930809
$CHCl_3$	-1417.6216537	-1417.8483758	-1417.9174349	-1417.9573443
CCl_4	-1876.6902682	-1876.9758053	-1877.0645012	-1877.1155513

Table A.4: Energies calculated for chloromethane molecules at CCSD(T) level from optimised CCSD(T)/AVTZ geometries.

	zpe	CCSD(T) E_h (Hartree)			
	(kJ mol^{-1})	DZ	TZ	QZ	CBS
CH_3Cl	99.52	-499.4716415	-499.5778793	-499.6080576	-499.6255652
CH_2Cl_2	77.71	-958.5482742	-958.7148054	-958.7643379	-958.7930566
$CHCl_3$	52.86	-1417.6221459	-1417.8484973	-1417.9174427	-1417.9572987

Table A.5: Energies calculated for bare halides and halogens at M06-2X/6-311++G(3df,3pd), MP2 and CCSD(T) levels.

	M06-2X E_h (Hartree)	MP2 E_h (Hartree)			CCSD(T) E_h (Hartree)			
		QZ	5Z	CBS	DZ	TZ	QZ	CBS
Br^-	-2574.2567261	-415.8967875	-415.9841607	-416.0757445	-415.7264356	-415.8364248	-415.9123563	-415.9599330
Br	-2574.1298719	-415.7667894	-415.8526493	-415.9425773	-415.6061898	-415.7132792	-415.7853280	-415.8302314
I^-	-	-295.0462742	-295.1063201	-295.1692937	-294.8832577	-294.9822875	-295.0612422	-295.1101157
I	-	-294.9223506	-294.9806967	-295.0417942	-294.7690618	-294.8654128	-294.9399754	-294.9859546

Table A.6: Energies calculated for bromide chloromethane anion complexes at M06-2X/6-311++G(3df,3pd) level from optimised M06-2X/6-31+G(d,p) geometries.

Complex	Interaction	zpe (kJ mol^{-1})	Corrected zpe (kJ mol^{-1})	M06-2X E_h (Hartree)
$Br^- \cdots CH_3Cl$	ID	101.06	1.81	-3074.3733075
	XB	100.64	1.36	-3074.3552440
$Br^- \cdots CH_2Cl_2$	HB	79.33	1.25	-3533.9758449
	XB	78.83	1.23	-3533.9617566
$Br^- \cdots CHCl_3$	HB	53.25	1.27	-3993.5762547
	XB	53.93	1.23	-3993.5627178
	IID	54.99	1.30	-3993.5549446
$Br^- \cdots CCl_4$	XB	26.29	1.18	-4453.1561258
	IID	27.12	1.24	-4453.1491193

Table A.7: Energies calculated for bromine chloromethane complexes at M06-2X/6-311++G(3df,3pd) level from optimised M06-2X/6-31+G(d,p) anion geometries.

Complex	Interaction	M06-2X E_h (Hartree)
$\mathrm{Br}\cdots\mathrm{CH_3Cl}$	ID	-3074.2294378
	XB	-3074.2304824
$\mathrm{Br}\cdots\mathrm{CH_2Cl_2}$	HB	-3533.8265735
	XB	-3533.8286498
$\mathrm{Br}\cdots\mathrm{CHCl_3}$	HB	-3993.4207674
	XB	-3993.4246072
	IID	-3993.4270707
$\mathrm{Br}\cdots\mathrm{CCl_4}$	XB	-4453.0105564
	IID	-4453.0158351

Table A.8: Energies calculated for halide chloromethane anion complexes at MP2 level from optimised MP2/AVQZ geometries.

Complex	Interaction	zpe (kJ mol^{-1})	Corrected zpe (kJ mol^{-1})	MP2 E_h (Hartree)		
				QZ	5Z	CBS
$\mathrm{Br^-}\cdots\mathrm{CH_3Cl}$	ID	101.24	1.41	-915.4772482	-915.5762296	-915.6789083
	XB	100.98	1.15	-915.4593576	-915.5587695	-915.6619547
$\mathrm{Br^-}\cdots\mathrm{CH_2Cl_2}$	HB	78.74	1.48	-1374.6196457	-1374.7265884	-1374.8372899
	XB	79.00	1.18	-1374.6037470	-1374.7108599	-1374.8217149
$\mathrm{Br^-}\cdots\mathrm{CHCl_3}$	HB	52.52	1.18	-1833.7607034	-1833.8753461	-1833.9937033
	XB	53.83	1.17	-1833.7445812	-1833.8595168	-1833.9781545
	IID	54.03	0.85	-1833.7356142	-1833.8505824	-1833.9690981
$\mathrm{Br^-}\cdots\mathrm{CCl_4}$	XB	26.28	1.21	-2292.8796613	-2293.0024955	-2293.1289854
	IID	26.44	0.83	-2292.8706459	-2292.9936106	-2293.1202508
$\mathrm{I^-}\cdots\mathrm{CCl_4}$	XB	26.12	1.02	-2172.0266658	-2172.1225013	-2172.2207266
	IID	26.32	0.69	-2172.0194091	-2172.1153835	-2172.2137666

Table A.9: Energies calculated for halogen chloromethane complexes at MP2 level from optimised MP2/AVQZ anion geometries.

Complex	Interaction	MP2 E_h (Hartree)		
		QZ	5Z	CBS
$\mathrm{Br\cdots CH_3Cl}$	ID	-915.3310428	-915.4286565	-915.5296610
	XB	-915.3314972	-915.4294044	-915.5309496
$\mathrm{Br\cdots CH_2Cl_2}$	HB	-1374.4661645	-1374.5715727	-1374.6805919
	XB	-1374.4674302	-1374.5739347	-1374.6829035
$\mathrm{Br\cdots CHCl_3}$	HB	-1833.6009693	-1833.7140749	-1833.8307473
	XB	-1833.6013282	-1833.7147008	-1833.8316383
	IID	-1833.6047368	-1833.7182489	-1833.8351106
$\mathrm{Br\cdots CCl_4}$	XB	-2292.7297589	-2292.8510122	-2292.9757849
	IID	-2292.7343823	-2292.8557800	-2292.9807088
$\mathrm{I\cdots CCl_4}$	XB	-2171.8879840	-2171.9820789	-2172.0783925
	IID	-2171.8924236	-2171.9866373	-2172.0830745

Table A.10: Energies calculated for halide chloromethane anion complexes at CCSD(T) level from optimised MP2/AVQZ geometries.

Complex	Interaction	CCSD(T) E_h (Hartree)			
		DZ	TZ	QZ	CBS
$\mathrm{Br^-\cdots CH_3Cl}$	ID	-915.2132009	-915.4302707	-915.5368165	-915.6021802
	XB	-915.1955754	-915.4128311	-915.5191690	-915.5843305
$\mathrm{Br^-\cdots CH_2Cl_2}$	HB	-1374.2958460	-1374.5730403	-1374.6984305	-1374.7747258
	XB	-1374.2790811	-1374.5567999	-1374.6826592	-1374.7591314
$\mathrm{Br^-\cdots CHCl_3}$	HB	-1833.3749713	-1833.7119045	-1833.8569045	-1833.9444764
	XB	-1833.3581701	-1833.6959626	-1833.8413616	-1833.9290381
	IID	-1833.3479924	-1833.6868340	-1833.8322388	-1833.9199544
$\mathrm{Br^-\cdots CCl_4}$	XB	-2292.4310341	-2292.8279295	-2292.9930608	-2293.0919230
	IID	-2292.4217879	-2292.8191662	-2292.9843177	-2293.0832397
$\mathrm{I^-\cdots CCl_4}$	XB	-2171.5848661	-2171.9709086	-2172.1392301	-2172.2394550
	IID	-2171.5773821	-2171.9640652	-2172.1322672	-2172.2324862

Table A.11: Energies calculated for halogen chloromethane complexes at CCSD(T) level from optimised MP2/AVQZ anion geometries.

Complex	Interaction	CCSD(T) E_h (Hartree)			
		DZ	TZ	QZ*	CBS
$Br\cdots CH_3Cl$	ID	-915.0773175	-915.2914462	-915.3939716	-915.4565641
	XB	-915.0777865	-915.2918286	-915.3944014	-915.4569919
$Br\cdots CH_2Cl_2$	HB	-1374.1529517	-1374.4267896	-1374.5482667	-1374.6218596
	XB	-1374.1530752	-1374.4286314	-1374.5496086	-1374.6232461
$Br\cdots CHCl_3$	HB	-1833.2263386	-1833.5595450	-1833.7006405	-1833.7855130
	XB	-1833.2255744	-1833.5600837	-1833.7015522	-1833.7865514
	IID	-1833.2283367	-1833.5632755	-	-1833.7897381
$Br\cdots CCl_4$	XB	-2292.2922164	-2292.6857264	-2292.8468542	-2292.9429996
	IID	-2292.2968849	-2292.6903050	-	-2292.9475616
$I\cdots CCl_4$	XB	-2171.4571974	-2171.8403090	-2172.0042044	-2172.1015397
	IID	-2171.4620185	-2171.8447779	-	-2172.1056977

*Some values were not calculated at CCSD(T), but were calculated at CCSD. A CBS extrapolation was therefore still able to be performed at W1w

Table A.12: Energies calculated for halide chloromethane anion complexes at CCSD(T) level from optimised CCSD(T)/AVTZ geometries.

Complex	Interaction	zpe (kJ mol^{-1})	Corrected zpe (kJ mol^{-1})	CCSD(T) E_h (Hartree)			
				DZ	TZ	QZ	CBS
$Br^-\cdots CH_3Cl$	ID	99.94	1.29	-915.2149840	-915.4309716	-915.5373564	-915.6026456
	XB	99.70	1.00	-915.1962811	-915.4130479	-915.5192337	-915.5843224
$Br^-\cdots CH_2Cl_2$	HB	78.20	1.36	-1374.2965856	-1374.5733036	-1374.6985384	-1374.7747516
	XB	78.15	1.08	-1374.2799045	-1374.5570354	-1374.6827325	-1374.7591324
$Br^-\cdots CHCl_3$	HB	52.58	1.15	-1833.3760531	-1833.7123367	-1833.8570610	-1833.9444811
	XB	53.33	1.09	-1833.3592683	-1833.6963133	-1833.8415095	-1833.9290940

Table A.13: Energies calculated for halogen chloromethane complexes at CCSD(T) level from optimised CCSD(T)/AVTZ anion geometries.

Complex	Interaction	CCSD(T) E_h (Hartree)			
		DZ	TZ	QZ	CBS
$Br\cdots CH_3Cl$	ID	-915.0787344	-915.2922005	-915.3941437	-915.4565542
	XB	-915.0787046	-915.2922977	-915.3947193	-915.4572348
$Br\cdots CH_2Cl_2$	HB	-1374.1544137	-1374.4278235	-1374.5491271	-1374.6226247
	XB	-1374.1542171	-1374.4283152	-1374.5501757	-1374.6239659
$Br\cdots CHCl_3$	HB	-1833.2287973	-1833.5614254	-1833.7022289	-1833.7869383
	XB	-1833.2272346	-1833.5610425	-1833.7023131	-1833.7872209

Table A.14: Vibrational frequencies and intensities of bare chloromethane molecules at M06-2X/6-31+G(d,p), MP2/AVQZ and CCSD(T)/AVTZ levels.

		M06-2X		MP2		CCSD(T)	
	Symmetry	Frequency (cm^{-1})	Intensity ($\mathrm{km\ mol}^{-1}$)	Frequency (cm^{-1})	Intensity ($\mathrm{km\ mol}^{-1}$)	Frequency (cm^{-1})	Intensity ($\mathrm{km\ mol}^{-1}$)
CH_3Cl	A_1	3105	21.4	3101	21.1	3075	23.1
	A_1	1405	16.0	1398	10.7	1391	12.0
	A_1	768	29.0	764	23.7	741	23.1
	E	3212	3.6	3214	2.0	3176	4.1
	E	3212	3.6	3214	2.0	3176	4.1
	E	1491	6.7	1507	5.9	1500	5.1
	E	1491	6.6	1507	5.9	1500	5.1
	E	1040	3.8	1049	2.1	1039	1.7
	E	1040	3.8	1049	2.1	1039	1.7
CH_2Cl_2	A_1	3170	5.5	3144	4.3	3124	5.9
	A_1	1477	0.0	1486	0.1	1484	0.0
	A_1	722	14.3	740	10.6	724	10.3
	A_1	285	0.7	289	0.4	285	0.4
	A_2	1201	0.0	1195	0.0	1189	0.0
	B_1	3181	1.2	3227	0.9	3199	0.1
	B_1	925	1.3	921	1.2	914	1.0
	B_2	1317	40.6	1303	37.2	1301	38.7
	B_2	762	135.4	791	121.4	773	116.4
$CHCl_3$	A_1	3214	0.8	3190	2.0	3177	0.8
	A_1	684	6.3	692	3.5	681	3.5
	A_1	378	0.5	375	0.2	370	0.2
	E	1263	26.4	1251	20.2	1254	21.2
	E	1262	26.9	1251	20.2	1254	21.2
	E	802	165.4	799	134.3	788	125.9
	E	802	167.1	799	134.3	788	125.9
	E	267	0.2	265	0.0	263	0.0
	E	267	0.2	265	0.0	263	0.0
CCl_4	A_1	468	0.0	472	0.0	-	-
	E	218	0.0	221	0.0	-	-
	E	218	0.0	221	0.0	-	-
	T_2	787	171.4	806	135.7	-	-
	T_2	787	171.4	806	135.7	-	-
	T_2	787	171.4	806	135.7	-	-
	T_2	318	0.0	321	0.0	-	-
	T_2	318	0.0	321	0.0	-	-
	T_2	318	0.0	321	0.0	-	-

Table A.15: Vibrational frequencies and intensities of bromide monochloromethane anion complexes at M06-2X/6-31+G(d,p), MP2/AVQZ and CCSD(T)/AVTZ levels.

		M06-2X		MP2		CCSD(T)	
	Symmetry	Frequency (cm^{-1})	Intensity ($km\ mol^{-1}$)	Frequency (cm^{-1})	Intensity ($km\ mol^{-1}$)	Frequency (cm^{-1})	Intensity ($km\ mol^{-1}$)
ID	A_1	3142	12.7	3144	6.3	3112	7.8
	A_1	1339	11.8	1339	7.8	1330	9.8
	A_1	639	170.6	685	115.4	651	123.2
	A_1	98	9.3	90	9.2	86	9.6
	E	3265	0.1	3270	0.1	3226	0.1
	E	3264	0.1	3270	0.1	3226	0.1
	E	1469	7.0	1484	3.3	1478	2.8
	E	1469	7.1	1484	3.3	1478	2.8
	E	1003	1.2	1007	2.2	996	1.7
	E	1003	1.2	1007	2.2	996	1.7
	E	103	6.4	73	5.6	65	5.5
	E	101	6.3	73	5.6	65	5.5
XB	A_1	3077	57.2	3086	67.5	3049	65.9
	A_1	1394	32.2	1382	18.6	1379	20.4
	A_1	767	0.0	773	0.8	748	1.3
	A_1	66	10.3	59	10.7	48	10.0
	E	3170	18.9	3187	13.2	3137	16.8
	E	3170	19.0	3187	13.2	3137	16.8
	E	1491	3.4	1506	3.9	1500	3.3
	E	1491	3.4	1506	3.9	1500	3.3
	E	1021	3.5	1032	0.9	1026	0.7
	E	1020	3.5	1032	0.9	1026	0.7
	E	81	1.8	67	1.6	60	1.5
	E	80	1.7	67	1.6	60	1.5

Table A.16: Vibrational frequencies and intensities of bromide dichloromethane anion complexes at M06-2X/6-31+G(d,p), MP2/AVQZ and CCSD(T)/AVTZ levels.

		M06-2X		MP2		CCSD(T)	
	Symmetry	Frequency	Intensity	Frequency	Intensity	Frequency	Intensity
		(cm^{-1})	(km mol^{-1})	(cm^{-1})	(km mol^{-1})	(cm^{-1})	(km mol^{-1})
HB	A'	3229	107.0	3205	41.7	3177	48.6
	A'	3119	287.2	2982	526.9	3014	394.6
	A'	1473	18.2	1482	17.0	1482	17.4
	A'	912	19.6	918	13.1	908	14.1
	A'	707	56.4	719	47.0	700	46.7
	A'	292	2.8	293	2.4	287	2.1
	A'	109	15.3	136	15.0	121	14.3
	A'	64	5.7	73	5.0	69	4.5
	A''	1359	71.3	1342	62.7	1335	65.1
	A''	1208	1.5	1210	0.5	1202	0.4
	A''	755	163.8	766	121.0	740	121.5
	A''	37	1.2	39	0.9	38	0.9
XB	A'	3140	20.0	3133	20.5	3107	21.1
	A'	1471	0.4	1482	0.1	1477	0.2
	A'	1310	83.7	1288	56.3	1285	56.7
	A'	765	51.9	788	47.2	765	42.3
	A'	707	65.6	719	56.6	697	59.6
	A'	282	10.8	288	7.5	282	7.4
	A'	82	18.1	78	17.4	69	16.3
	A'	44	0.6	45	1.3	41	1.5
	A''	3218	2.2	3212	0.8	3182	1.4
	A''	1187	0.1	1186	0.0	1181	0.0
	A''	894	1.0	912	0.4	909	0.2
	A''	78	2.1	75	1.8	70	1.7

Table A.17: Vibrational frequencies and intensities of bromide trichloromethane anion complexes at M06-2X/6-31+G(d,p), MP2/AVQZ and CCSD(T)/AVTZ levels.

		M06-2X		MP2		CCSD(T)	
	Symmetry	Frequency (cm^{-1})	Intensity (km mol^{-1})	Frequency (cm^{-1})	Intensity (km mol^{-1})	Frequency (cm^{-1})	Intensity (km mol^{-1})
HB	A_1	2865	1254.3	2790	1241.7	2873	1026.9
	A_1	665	76.2	670	56.6	660	52.9
	A_1	382	6.6	380	4.7	373	3.6
	A_1	104	14.9	106	14.9	101	14.3
	E	1340	47.4	1323	43.7	1321	44.3
	E	1340	47.5	1323	43.7	1321	44.3
	E	784	167.4	783	125.3	764	121.3
	E	784	169.0	782	125.3	764	121.3
	E	266	0.0	265	0.0	262	0.0
	E	266	0.0	265	0.0	262	0.0
	E	54	0.8	46	0.6	45	0.6
	E	54	0.8	46	0.6	45	0.6
XB	A'	3198	0.9	3180	0.9	3165	1.1
	A'	1251	40.8	1236	33.6	1239	26.0
	A'	778	53.9	795	50.3	783	45.3
	A'	675	29.4	683	25.8	670	26.0
	A'	365	19.2	368	14.1	362	14.4
	A'	262	11.2	262	7.7	259	7.1
	A'	90	20.0	85	21.4	78	20.1
	A'	64	2.2	61	3.3	57	3.4
	A''	1252	31.4	1245	24.5	1245	26.0
	A''	759	193.8	762	154.3	743	148.9
	A''	272	0.1	274	0.1	269	0.1
	A''	51	0.8	49	0.6	47	0.6
IID	A_1	3191	3.0	3183	0.2	-	-
	A_1	678	9.4	687	4.5	-	-
	A_1	381	0.7	369	0.6	-	-
	A_1	74	10.0	52	10.7	-	-
	E	1285	23.3	1255	15.6	-	-
	E	1284	23.7	1255	15.6	-	-
	E	809	153.4	809	122.3	-	-
	E	809	156.0	809	122.3	-	-
	E	270	0.0	262	0.0	-	-
	E	270	0.0	262	0.0	-	-
	E	72	0.0	45	0.1	-	-
	E	72	0.0	45	0.1	-	-

Table A.18: Vibrational frequencies and intensities of bromide tetrachloromethane anion complexes at M06-2X/6-31+G(d,p) and MP2/AVQZ levels.

		M06-2X		MP2	
	Symmetry	Frequency (cm^{-1})	Intensity ($\mathrm{km\ mol}^{-1}$)	Frequency (cm^{-1})	Intensity ($\mathrm{km\ mol}^{-1}$)
XB	A_1	785	21.1	782	24.2
	A_1	446	46.8	448	34.0
	A_1	308	37.7	307	26.7
	A_1	86	30.8	86	33.2
	E	783	196.9	778	155.3
	E	782	198.0	778	155.3
	E	321	0.3	324	0.4
	E	321	0.3	324	0.4
	E	225	0.1	225	0.0
	E	225	0.1	225	0.0
	E	56	0.8	58	0.6
	E	55	0.8	58	0.6
IID	A_1	744	227.8	757	178.3
	A_1	473	2.9	475	2.2
	A_1	321	1.7	313	1.1
	A_1	75	12.0	56	12.3
	E	834	149.3	825	116.3
	E	833	151.3	825	116.3
	E	330	0.0	323	0.0
	E	330	0.0	323	0.0
	E	229	0.3	221	0.1
	E	229	0.3	221	0.1
	E	66	1.1	41	1.0
	E	66	1.1	41	1.0

Table A.19: Vibrational frequencies and intensities of iodide tetrachloromethane anion complexes at MP2/AVQZ.

		MP2	
	Symmetry	Frequency (cm^{-1})	Intensity (km mol^{-1})
XB	A_1	783	27.7
	A_1	450	32.8
	A_1	308	22.6
	A_1	68	17.3
	E	782	152.5
	E	782	152.5
	E	323	0.2
	E	323	0.2
	E	224	0.0
	E	224	0.0
	E	51	0.2
	E	51	0.2
IID	A_1	764	184.3
	A_1	475	1.8
	A_1	314	0.8
	A_1	45	5.9
	E	823	108.5
	E	823	108.6
	E	323	0.0
	E	323	0.0
	E	221	0.1
	E	221	0.1
	E	35	0.3
	E	35	0.3

Table A.20: Cartesian coordinates of the geometries of bare chloromethane molecules optimised at MP2/AVQZ, in Å.

Atom	x	y	z
C	0.00000	0.00000	-1.12200
H	0.00000	1.02848	-1.46483
H	0.89069	-0.51424	-1.46483
H	-0.89069	-0.51424	-1.46483
Cl	0.00000	0.00000	0.65450
C	0.00000	0.00000	0.76690
H	-0.89608	0.00000	1.37478
H	0.89608	0.00000	1.37478
Cl	0.00000	1.46455	-0.21621
Cl	0.00000	-1.46455	-0.21621
C	0.00000	0.00000	0.45955
H	0.00000	0.00000	1.54170
Cl	0.00000	1.67359	-0.08429
Cl	1.44937	-0.83680	-0.08429
Cl	-1.44937	-0.83680	-0.08429
C	0.00000	0.00000	0.00000
Cl	1.01810	1.01810	1.01810
Cl	-1.01810	-1.01810	1.01810
Cl	1.01810	-1.01810	-1.01810
Cl	-1.01810	1.01810	-1.01810

Table A.21: Cartesian coordinates of the geometries of bare chloromethane molecules optimised at CCSD(T)/AVTZ, in Å.

Atom	x	y	z
C	-1.22995524	0.00000000	0.00000000
H	-1.57085600	0.51592330	-0.89360537
H	-1.57085600	-1.03184660	0.00000000
H	-1.57085600	0.51592330	0.89360537
Cl	0.55789382	0.00000000	0.00000000
C	0.00000000	0.00000000	-0.80859414
H	0.89837813	0.00000000	-1.41586557
H	-0.89837837	0.00000000	-1.41586520
Cl	0.00000000	1.47293420	0.17954576
Cl	0.00000000	-1.47293420	0.17954577
C	-0.47606499	0.00000000	0.00000000
H	-1.55873748	0.00000000	0.00000000
Cl	0.06943050	-0.84126340	-1.45711096
Cl	0.06943050	1.68252681	0.00000000
Cl	0.06943050	-0.84126340	1.45711096

Table A.22: Cartesian coordinates of the geometries of bromide monochloromethane complexes optimised at MP2/AVQZ, in Å.

Atom	Ion Dipole			Halogen Bond		
	x	y	z	x	y	z
C	0.00000	0.00000	-1.38310	0.00000	0.00000	-3.44884
H	0.00000	1.01408	-1.04563	0.00000	1.02377	-3.80891
H	0.87822	-0.50704	-1.04563	-0.88661	-0.51188	-3.80891
H	-0.87822	-0.50704	-1.04563	0.88661	-0.51188	-3.80891
Cl	0.00000	0.00000	-3.17823	0.00000	0.00000	-1.67949
Br	0.00000	0.00000	1.87044	0.00000	0.00000	1.73346

Table A.23: Cartesian coordinates of the geometries of bromide monochloromethane complexes optimised at CCSD(T)/AVTZ, in Å.

Atom	Ion Dipole			Halogen Bond		
	x	y	z	x	y	z
C	1.51667393	0.00000000	0.00000000	-3.73620707	0.00000000	0.00000000
H	1.17698653	-0.51436556	-0.89090729	-4.09346636	0.51446587	-0.89108103
H	1.17698653	1.02873112	0.00000000	-4.09346636	-1.02893174	0.00000000
H	1.17698653	-0.51436556	0.89090729	-4.09346636	0.51446587	0.89108103
Cl	3.33936205	0.00000000	0.00000000	-1.95352235	0.00000000	0.00000000
Br	-1.75538846	0.00000000	0.00000000	1.59054815	0.00000000	0.00000000

Table A.24: Cartesian coordinates of the geometries of bromide dichloromethane complexes optimised at MP2/AVQZ, in Å.

Atom	Hydrogen Bond			Halogen Bond		
	x	y	z	x	y	z
C	-0.98258	-0.75750	0.00000	0.40836	2.43450	0.00000
H	-0.10428	-0.10171	0.00000	0.01365	2.90357	0.89287
H	-1.89731	-0.18007	0.00000	0.01365	2.90357	-0.89287
Cl	-0.98258	-1.76083	1.45980	0.00000	0.73460	0.00000
Cl	-0.98258	-1.76083	-1.45980	2.16633	2.74619	0.00000
Br	1.18014	1.84843	0.00000	-1.12300	-2.27393	0.00000

Table A.25: Cartesian coordinates of the geometries of bromide dichloromethane complexes optimised at CCSD(T)/AVTZ, in Å.

Atom	Hydrogen Bond			Halogen Bond		
	x	y	z	x	y	z
C	0.43090020	1.28281363	0.00000000	2.51441546	-0.87140449	0.00000000
H	1.51412204	1.23936784	0.00000000	2.71940467	-1.44042675	0.90105028
H	-0.00283418	0.27753387	0.00000000	2.71940467	-1.44042675	-0.90105028
Cl	-0.07600282	2.15424518	-1.47296542	3.65933968	0.51654419	0.00000000
Cl	-0.07600282	2.15424518	1.47296542	0.82215740	-0.38050616	0.00000000
Br	-0.01746684	-2.12353058	0.00000000	-2.43754714	0.10901340	0.00000000

Table A.26: Cartesian coordinates of the geometries of bromide trichloromethane complexes optimised at MP2/AVQZ, in Å.

Atom	Hydrogen Bond			Halogen Bond			Ion Induced Dipole		
	x	y	z	x	y	z	x	y	z
C	-0.93869	0.00000	0.00000	-1.53707	-1.08648	0.00000	0.01792	0.17572	-1.74077
H	0.17112	0.00000	0.00000	-2.48030	-0.55583	0.00000	0.02893	0.28369	-2.81045
Cl	-1.51014	-0.10336	-1.66541	-0.21766	0.05134	0.00000	1.33797	-0.88943	-1.29870
Cl	-1.51014	1.49397	0.74319	-1.53707	-2.11535	-1.44831	-1.52957	-0.51333	-1.29025
Cl	-1.51014	-1.39060	0.92222	-1.53707	-2.11535	1.44831	0.22898	1.76923	-1.04175
Br	2.35652	0.00000	0.00000	1.93324	2.23211	0.00000	-0.02205	-0.21623	2.14220

Table A.27: Cartesian coordinates of the geometries of bromide trichloromethane complexes optimised at CCSD(T)/AVTZ, in Å.

Atom	Hydrogen Bond			Halogen Bond		
	x	y	z	x	y	z
C	-1.04575853	0.00000000	0.00000000	0.50644919	1.96728419	0.00000000
H	0.05896114	0.00000000	0.00000000	1.57295167	2.15626471	0.00000000
Cl	-1.62208932	0.84037312	-1.45556895	0.20791806	0.23951542	0.00000000
Cl	-1.62208932	-1.68074625	0.00000000	-0.15227439	2.76782989	1.45866005
Cl	-1.62208932	0.84037312	1.45556895	-0.15227439	2.76782989	-1.45866005
Br	2.31451265	0.00000000	0.00000000	-0.05427871	-2.88566396	0.00000000

Table A.28: Cartesian coordinates of the geometries of halide tetrachloromethane complexes optimised at MP2/AVQZ, in Å.

Atom	Halogen Bond			Ion Induced Dipole		
	x	y	z	x	y	z
C	0.00000	0.00000	-1.48119	0.00000	-1.22067	0.00000
Cl	0.00000	1.66041	-2.11261	0.00000	-3.01094	0.00000
Cl	1.43796	-0.83021	-2.11261	1.65911	-0.66307	0.00000
Cl	-1.43796	-0.83021	-2.11261	-0.82956	-0.66307	1.43684
Cl	0.00000	0.00000	0.27226	-0.82956	-0.66307	-1.43684
Br	0.00000	0.00000	3.20006	0.00000	2.63790	0.00000
C	0.94575	0.88675	-1.57465	-1.72539	0.00000	0.00000
Cl	2.17071	2.03557	-1.00232	-3.51206	0.00000	0.00000
Cl	1.75193	-0.32850	-2.58515	-1.16252	-1.63069	-0.30188
Cl	-0.21519	1.76911	-2.58536	-1.16252	0.55391	1.56316
Cl	0.13194	0.12371	-0.21968	-1.16252	1.07678	-1.26128
I	-1.33857	-1.25507	2.22869	2.44049	0.00000	0.00000